Additive Manufacturing 48 (2021) 102447

Contents lists available at ScienceDirect

Additive Manufacturing

journal homepage: www.elsevier.com/locate/addma

Research paper

Harnessing light to create functional, three-dimensional polymeric materials: multitasking initiation systems as the critical key to success

Wiktoria Tomal [a], Dominika Krok [a], Anna Chachaj-Brekiesz [b], Petr Lepcio [c], Joanna Ortyl [a,d,e,*]

[a] Cracow University of Technology, Faculty of Chemical Engineering and Technology, Warszawska 24, 31–155 Cracow, Poland
[b] Jagiellonian University, Faculty of Chemistry, Gronostajowa 2, 30–387 Cracow, Poland
[c] Central European Institute of Technology, Brno University of Technology, Purkynova 656/123, Brno 612 00, Czech Republic
[d] Photo HiTech Ltd., Bobrzyńskiego 14, 30–348 Cracow, Poland
[e] Photo4Chem, Lea 114, 30-133 Cracow, Poland

ARTICLE INFO

Keywords:
Photoinitiating system
Photopolymerization
CNTs nanocomposites
Real-time FTIR
Photo-rheology
3D-VAT printing
DLP printing
Laser 3D printing

ABSTRACT

Nowadays, the lack of suitable photoinitiators (PI) and photoinitiating systems (PISs) represents the utmost challenge in 3D-VAT printing. High photoinitiating efficiency is needed for example in the presence of nanofillers such as carbon nanotubes (CNTs) which absorb and scatter light. Many prominent PISs contains iodonium salt as an initiator and a second component as a photosensitizer. This study addresses the high demand for innovative PISs with improved photoinitiating efficiency by a complete cycle of research: from the synthesis of new biphenyl derivatives, through their employment as photosensitizers of iodonium salt for light-induced cationic, free-radical, and hybrid polymerization processes, to the representative application in 3D printing processes such as digital light processing (DLP) or laser printing. The ultimate performance of the newly synthetized compounds was tested by preparing 3D-printable photosensitive nanocomposite resins filled with CNTs as a nanoscale filler. Their photopolymerization kinetics as well as the effect of the CNT concentration on the crosslinking were analyzed via real-time FTIR and photo-rheology. The printouts were observed with optical microscopy and scanning electron microscopy. In addition, the key printing parameters were determined, i.e. E_c (critical energy to initiate polymerization) and D_p (penetration depth of curing light). Our results evidence the capability of the synthetized compounds to take part in the photoinitiating systems of complex and demanding 3D printing applications.

1. Introduction

Light. Underestimated on a daily basis, but in fact essential to every human being. Light is a key element in our lives and has been used since the time begun to maintain health, or to work productively after dark. Light is also the excellent "substrate" for many processes used extensively in various areas of life and science. One of the process that has taken science and industry by storm is light-initiated polymerization process, so called photopolymerization [1–6]. This type of polymerization has been widely used in the coating industry, in the polygraphic industry or for the production of solvent-free paints, varnishes and adhesives [7,8]. On the other hand, photopolymerization is widely used in the medical industry [9], e.g. in dentistry to fill dental cavities [10], for targeted drug therapy [11] or in materials engineering to produce hydrogel materials [12–14]. Numerous advantages of this process such as no need for solvents, short reaction times, and conducting the reaction at room temperature make photopolymerization a significant contribution to the development of these fields. One technology that increasingly combines polymerization processes and light is 3D printing [15–18]. So called 3D-VAT printing is one of the methods of additive manufacturing, which, due to the unprecedented shape control and lack of need for molds and mechanical processing of objects, is considered to be one of the most advanced methods of material production [19–27]. 3D printing techniques based on photopolymerization, such as stereolithography (SLA) or digital light processing (DLP) are currently attracting much attention due to their versatility and customizability [28,29]. They are characterized by a number of advantages: high spatio-temporal control over the process, production of materials with a well-defined geometry and high optical resolution, while maintaining reasonable material build rates.

* Corresponding author at: Cracow University of Technology, Faculty of Chemical Engineering and Technology, Warszawska 24, 31–155 Cracow, Poland.
E-mail address: jortyl@pk.edu.pl (J. Ortyl).

https://doi.org/10.1016/j.addma.2021.102447
Received 21 July 2021; Received in revised form 27 October 2021; Accepted 27 October 2021
Available online 5 November 2021

Composite materials are a class of multifunctional materials that are immensely popular due to their beneficial properties. Particularly noteworthy are nanocomposite materials, in which the addition of a filler with a dimension at the nanoscale significantly changes the final properties of the product, such as improves its thermo-mechanical properties [30–32], increases heat resistance, provides conductive properties and many others. The final properties depend on the selection of a suitable nanofiller, of which the widely used additives are carbon nanotubes (CNTs) [33–35], silica [36–39], aluminum oxides [40], clays [41], natural [42] and polymeric fibers [43]. Standard additive methods for obtaining composite materials focus on techniques such as PolyJet, Binder Jetting, FDM, etc., which are dedicated to materials of significant size without the possibility of precise spatio-temporal control over the resin curing process [35,44]. The use of the photopolymerization technique makes it possible to print nanocomposite materials of desired geometries, at reasonable printing rates, with no need of further mechanical processing of the finished element [45–48]. Although 3D-VAT printing techniques are in the scientific spotlight, the fabrication of nanocomposite materials using SLA or DLP printing is still flawed. The presence of a filler often reduces the speed of the photopolymerization process and hinders the fabrication of the final material, due to, inter alia, the self-agglomeration of the nano-additive in the resin, or the fact that dark fillers absorb light and light fillers scatter light, making it difficult for the light to act uniformly on the sample. Moreover, these effects further depend on the spatial arrangement of nanoparticles which, in a liquid medium, is controlled by a complex balance of forces [49,50]. Therefore, finding the right composition of a photo-curable resin: monomer/monomers, initiating system, additives, as well as adjusting the right 3D printing conditions is constantly a topic of work for researchers around the world.

The numerous difficulties caused by the presence of nanometric filler in the resin make the fabrication of nanocomposite materials via techniques such as DLP still a challenge for both the scientific and industrial environments. In the course of research, we have demonstrated that the use of a suitable initiating system plays a key role in photopolymerization processes and can extend the application capabilities of raw materials in which it is used. In the previous work, we have reported on a series of biphenyl derivatives as iodonium salt sensitizers, in order to find effective photoinitiating system for various light induced polymerization processes. The first group of biphenyl derivatives were 2-amino-4-methyl-6-phenyl-benzene-1,3-dicarbonitrile derivatives, which efficiently initiated various photopolymerization processes in particular using light in the soft UV range – @365 nm, but also enabled high resolution printing using laser engraver [51]. In another approach, we decided to replace the chromophore of the biphenyl derivatives and introduced derivatives named: 2-(diethylamino)−4-(1-ethylpropyl)−6-phenyl-benzene-1,3-dicarbonitrile derivatives [52]. The incorporation of diethylamine in positions two provided an improved absorbance spectrum of these compounds, which in turn provided higher initiation efficiency at 405 nm.

However, in the search for an "ideal" initiation system, we decided to use a third group of derivatives: 2-(diethylamino)−4-methyl-6-heteroarylbenzene-1,3-dicarbonitriles to investigate how the proposed chromophore affects the photosensibilizing properties of these compounds. Thus, three groups of biphenyl derivatives characterized by three different chromophores and six different substituents have been compared in this study, in terms of their spectroscopic, electrochemical and thermodynamic properties. Subsequently, the performance of these derivatives in free-radical, cationic and hybrid photopolymerization reactions was investigated by forming IPN-type networks. With the example of previous derivatives, we have also analyzed the initiation mechanism of these two-component initiating systems under photoreduction cycle with amine as a co-initiator and photo-oxidation with iodonium salt as a photoinitiator. This extensive research has led to the employment of selected biphenyl derivatives in a two-component initiating system dedicated to photosensitive polymer resins for 3D printing, including carbon nanotube-containing nanoresins. The effect of the nanofiller on the kinetics of the photopolymerization process was analyzed using real-time FT-IR and photo-rheology, which was crucial for improved selection of the resin composition and optimization of the printing parameters itself. In addition, key printing parameters were determined, i.e. E_c (critical energy to initiate polymerization) and D_p (penetration depth of curing light). We have demonstrated the feasibility of preparing photosensitive resins containing biphenyl–iodonium salt initiating system and printing CNTs nanocomposite materials of significant dimensions using digital light processing-based printing (DLP), and we have characterized the finished printouts using optical microscopy and scanning electron microscopy.

The increased interest in light-based additive technologies, or so-called 3D-VAT printing, has caused researchers to continually search for suitably efficient initiating systems for use in this process. However, in the case of using additive technologies for the production of nanocomposite materials, most of the scientific articles focus on the introduction of a nano-additive into a commercial resin and on the study of the properties of the finished material, while the initiation process itself is pushed into the background. Some articles focus also on the selection of the initiator itself and the most commonly used are phosphine oxide derivatives such as: (2,4,6-trimethyl benzoyl diphenyl phosphine oxide) (TPO) or bis(2,4,6-trimethylbenzoyl)-phosphineoxide (BAPO) [53–55]. Gonzalez, et al. demonstrated in their work on the manufacturing of three-dimensional nanocomposites containing CNTs that the use of BAPO initiator in amounts up to 6% by weight, does not achieve the desired level of monomer conversion and the conversion stops at about 80% [56]. It is worth mentioning that the necessity to use BAPO even at the level of 3% by weight causes numerous problems with the miscibility of photosensitive resin with photoinitiator and causes numerous technological problems. Two-component initiating systems for 3D printing applications have also been reported in the literature, but they mainly focus on printing with resins that do not contain nano-additives, and finding a suitable fast two-component initiating system to obtain 3D nano-materials using a commercial DLP 3D printer with low intensity visible LEDs is still an ongoing research topic [57–59]. Despite the recent developments in high-efficiency photoinitiators [22,60], the newly synthesized compounds presented in this work push the performance of photoinitiation and photopolymerization processes to an even higher level. Their implementation in 3D printing allows, among others, to reduce the processing time, print thicker layers up to a millimeter range, or improve the printing accuracy even for nanocomposites with a high content of wide-range absorbing nanofillers such as carbon nanotubes. Our study also proves the feasibility of printing viscous resins without the need for lowering the viscosity with reactive diluents, which further extends the versatility of this additive manufacturing technique and effectively oppose the increased viscosity often accompanying the addition of nanofillers.

2. Experiments

2.1. Materials

Three series of biphenyl derivatives were investigated for the role of photosensitizer in various photopolymerization reactions and ultimately for use in 3D printing techniques. The A, B, and C series contained derivatives based on a single chromophore in each group, but with different substituents (Fig. 1, columns). The derivatives in the rows (Fig. 1) had the same substituents but differed in the chromophore. The full names of all derivatives from the A, B, and C series are listed in the Supplementary Information while their structures are displayed in the Fig. 1. A detailed information regarding the synthesis of the biphenyl derivatives as well as the results of ^{13}C NMR, ^{1}H NMR analyses are summarized in the Supplementary Information (Figs. S1–S17).

The following components were used for the initiation reaction: iodonium salt Speedcure 938: bis-(4-t-butylphenyl)iodonium

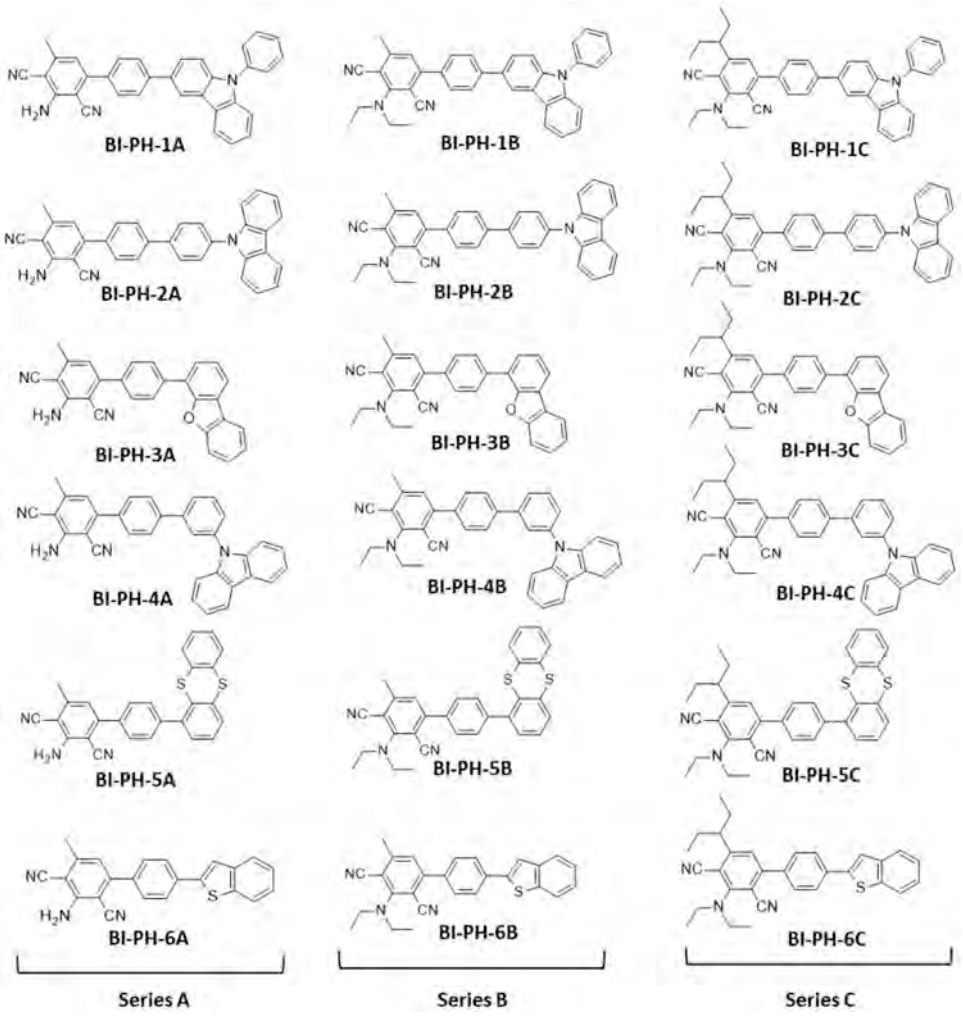

Fig. 1. Structures of biphenyl derivatives investigated with this study: series A - 2-amino-4-methylbenzene-6-heteroaryl-1,3-dicarbonitriles; series B - 2-(diethylamino)−4-methyl-6-heteroarylbenzene-1,3-dicarbonitriles; series C - 2-(diethylamino)−4-(1-ethylpropyl)− 6-heteroarylbenzene-1,3-dicarbonitriles.

hexafluorophosphate (IOD, from Lambson Ltd., Wetherby, UK) as a commercial photoinitiator or 2) with methyl diethanolamine (MDEA, Sigma Aldrich) as a co-initiator in type-II photoinitiating systems. In addition, 2,4-diethyl-9 H-thioxanthen-9-one (DETHX, from Sigma Aldrich) was applied as a commercial sensitizer. Two types of monomers were used for the standard investigation of light induced polymerization processes: trimethylolpropane triacrylate (TMPTA, from Sigma Aldrich) for free-radical photopolymerization and 3,4-epoxycyclohexylmethyl-3,4-epoxycyclohexane-carboxylate (CADE, from Lambson Ltd., Wetherby, UK) for cationic photopolymerization. In addition, the following monomers were used for 3D printing applications: di(ethylene glycol) dimethacrylate (DEGDMA, from Sigma Aldrich), di(ethylene glycol) diacrylate (DEGDA, from Sigma Aldrich), 2-Hydroxyethyl methacrylate (HEMA, from Sigma Aldrich) and bisphenol A ethoxylate diacrylate (BEDA, from Sigma Aldrich). Multiwalled carbon nanotubes, NC7000™, for the nanocomposite formation were kindly provided by Nanocyl S.A. (Sambreville, Belgium). Structures of the used materials are shown in Fig. S18 in Supplementary Information.

2.2. Spectroscopic characteristics

2.2.1. Absorption properties

TEC-X2 spectrometer (from StellarNet, Inc., Tampa, FL, USA), equipped with a broadband SL5 Deuterium Halogen Light Source for UV–VIS (from StellarNet, Inc., Tampa, FL, USA), was used for the investigation of absorbance properties of biphenyl derivatives in acetonitrile, at 25 °C. Measurements were carried in quartz cuvette with the optical path of 10 mm.

2.2.2. Fluorescence quenching

FluoroMax-4P spectrofluorometer (Horiba, Kyoto, Japan) was utilized in order to investigate fluorescent quenching of the series A - 2-amino-4-methylbenzene-6-heteroaryl-1,3-dicarbonitriles; series B - 2-(diethylamino)−4-methyl-6-heteroarylbenzene-1,3-dicarbonitriles; series C - 2-(diethylamino)−4-(1-ethylpropyl)−6-heteroarylbenzene-1,3-dicarbonitriles in the presence of iodonium salt (IOD) at concentration: $2{,}7{\cdot}10^{-2}$ mol/dm^3.

2.2.3. Fluorescence lifetime

Spectrometer EasyLife™ (Fluorescence Lifetime Fluorometer by Photon Technology International (PTI), currently a part of Horiba) was used to record the fluorescence decay curves of biphenyl derivatives in acetonitrile. A pulsed LED at 310 nm was applied as a source light. Colloidal silica solution (MW 60.08) in water – Ludox® (from Sigma Aldrich) was used as a reference for these experiments, and the fluorescence lifetimes (τ) were estimated by fitting the decay curves via a deconvolution procedure available in the Fluorescence Decay Analysis Software.

2.3. Electrochemical characteristic determination of oxidation and reduction potential

Cyclic voltammetry was used to determine the oxidation (E_{ox} vs Ag/AgCl) and reduction potentials (E_{red} vs Ag/AgCl) of biphenyl derivatives from series A, B, and C. Electrochemical Analyzer M161 and the Electrode Stand M164, from MTM-ANKO, Cracow, Poland was equipped with tetrabutylammonium hexafluorophosphate (0.1 M) (from Sigma Aldrich) as a supporting electrolyte, a silver chloride electrode – Ag/AgCl as a reference and a platinum disc as the working electrode. Process parameters were: a scan rate of 0.1 V/s; ferrocene was used as a standard and the potentials were determined from the half peak potentials.

The Gibbs free energy ΔG_{et} for an electron transfer between the components of the photoinitiating system were calculated from the obtained oxidation and reduction potentials using the following formula:

$$\Delta G_{et} = F[E_{ox}\ (D/D^{\bullet+}) - E_{red}\ (A^{\bullet-}/A)] - E_{00} - (Ze^2/\varepsilon a) \quad (1)$$

where: E_{ox} ($D/D^{\bullet+}$) is oxidation potential of the electron donor, E_{red} ($A^{\bullet-}/A$) – the reduction potential of the electron acceptor, E_{00} – the excited state energy, ($Ze^2/\varepsilon a$) the electrostatic interaction energy for the initially formed ion pair. The parameter ($Ze^2/\varepsilon a$) is negligible in polar solvents. The excited state energy was determined from the excitation and emission spectra using a FluoroMax-4P spectrofluorometer (Horiba, Kyoto, Japan). All spectra were recorded at varied excitation wavelengths in the range of 200–800 nm.

2.4. Real-time FT-IR experiments

The kinetics of light induced polymerization processes was investigated using the real-time FT-IR method with FT-IR^{i10} NICOLET™ spectrometer with a horizontal adapter (from Thermo Scientific, Waltham, MA, USA). The compositions and quantities were determined based on the mass ratios of the initiating system components in relation to the amount of monomer/monomers used. Samples were prepared in a darkened room, where the only light source was red light. The monomer conversion can be determined based on the changes in the absorbance of the analyzed sample, namely the decrease in the absorbance of peaks responsible for functional groups or bonds involved in the curing process, using the following formula:

$$Conversion\ [\%] = \left(1 - \frac{Area_{\ after\ \ polymerization}}{Area_{\ before\ \ polymerization}}\right) * 100\ \ \% \quad (2)$$

The characteristic absorbance peaks for investigated monomers are described below in detail for each photopolymerization individually.

Since the employed photosensitizers - biphenyl derivatives had an absorption range reaching the visible region, the following light sources were used for photopolymerization studies: 405 nm M405L4 Vis-LED diode (CW=0,7 A, from Thorlabs Inc., Tampa, FL, USA) and 415 nm M415L4 Vis-LED diode (CW=0,7 A, from Thorlabs Inc., Tampa, FL, USA). The power of light was regulated by a DC2200 regulated power supply (from Thorlabs Inc., Tampa, FL, USA). The UV-LED was started with a 10 s delay from the start of the procedure. The distance between irradiation sources and formulations was 2.1 cm.

2.4.1. Cationic photopolymerization of epoxide monomer

The photocurable compositions consisted of epoxy monomer CADE and appropriate initiating system: IOD (1.0 wt%) and biphenyl derivatives (0.1 wt%). Amounts of photo-initiating systems were calculated according to the quantity of the used monomer. A mixture of iodonium salt (IOD; 1.0 wt%) and CADE monomer was used as a reference and as a second – commercial reference, two component photoinitiating system were applied: IOD (1.0 wt%) and DETHX (0.1 wt %) with CADE monomer. The experiments were carried out in laminated conditions (on the BaF_2 pallet; thickness 25 μm) and the epoxy content was continuously followed under air at about 790 cm^{-1} for 800 s

2.4.2. Free-radical photopolymerization of acrylate monomer

A mixture of the TMPTA acrylate monomer and a two-component initiating system: IOD (1.0 wt%) and biphenyl derivative (0.1 wt%) was investigated. Quantities of initiator system were recalculated relative to the amount of monomer used. As a reference a mixture of iodonium salt (IOD; 1.0 wt%) and TMPTA monomer was used, and as a second – commercial reference, two component photoinitiating system were applied: IOD (1.0 wt%) and DETHX (0.1 wt%) with TMPTA monomer. The laminated samples (between two polypropylene films; thickness 25 μm) were deposited on a horizontal holder for FT-IR spectrometer and were irradiated. The evolution of the double bond of acrylate was monitored at 1.635 cm^{-1} for 400 s

2.4.3. Hybrid photopolymerization of epoxide/acrylate mixture

The following resin was used for the formation of Interpenetrating Polymer Networks (IPNs): a mixture CADE epoxy monomer and TMPTA acrylate monomer in mass ratio 1:1, and a photo-initiating system consisted of biphenyl derivative (0.1 wt%) and IOD (1.0 wt%). The polymerization process was carried out under three measurement conditions: in air (on a BaF_2 pellet; sample thickness ~25 μm), in air (in the ring form; sample dimension: 1.5 mm thickness and 12 mm diameter), in laminate (between two polypropylene films, sample thickness ~25 μm). The double bond content of acrylate monomer was continuously followed at about 1.635 cm^{-1} and epoxy content – at about 790 cm^{-1} for 600 s

2.4.4. Free-radical photopolymerization with biphenyl/MDEA as type ii initiating system

Series A**:** 2-amino-4-methylbenzene-6-heteroaryl-1,3-dicarbonitriles**,** series B**:** 2-(diethylamino)−4-methyl-6-heteroarylbenzene-1,3-dicarbonitriles**,** series C**:** 2-(diethylamino)−4-(1-ethylpropyl)−6-heteroarylbenzene-1,3-dicarbonitriles (0.1 wt%), together with amine (MDEA) as co-initiator (1.5 wt%), were investigated as type II photoinitiating system dedicated for free-radical photopolymerization of acrylate monomer – TMPTA. The experiments were carried out in laminate conditions (between two polypropylene films; sample thickness 25 μm). The evaluation of double bond content was continuously monitored at about 1.635 nm^{-1} for 400 s

2.4.5. Free-radical photopolymerization during the formation of CNTs composites

For the MWCNTs composite formation following resins were prepared: selected biphenyl derivative of 2-(diethylamino)− 4-(1-ethylpropyl)− 6-(4-thianthren-1-ylphenyl)benzene-1,3-dicarbonitrile, BI-PH-5 C (0.2 wt%), IOD (2.0 wt.) and mixture of diacrylate monomers: DEGDA/DEGMA (1/1.5 wt%). Various MWCNTs content were used for this experiments: 0.1%; 0.25%; 0.5% and 1.0% (by weight). As a reference a mixture of iodonium salt/BI-PH-5 C (1/0.1 wt.) and monomers: DEGDA/DEGMA (1/1.5 wt%) was applied. The experiments were carried out in air, in the ring form, sample dimension: 1.5 mm thickness and 12 mm diameter. The content of double bond of methacrylate was followed between 6100 cm^{-1} and 6230 cm^{-1} for 600 s

2.5. 3D-VAT printing

2.5.1. Laser 3D printing

A Laser Engraver Printer machine (NEJE DK-8-KZ) was applied in order to obtain the laser write printout under laser source of light at 405 nm (spot diameter, ~75 μm). Various composition were examined: 1) BI-PH-5B (0.1 wt%) + IOD (1.0 wt%) + mixture of monomers: CADE/TMPTMA (1/1 wt.) (laser intensity: 100 mW/cm^2); 2) BI-PH-5B (0.1 wt%) + IOD (1.0 wt%) + mixture of monomers: CADE/TMPTMA (1/1 wt.) (laser intensity: 100 mW/cm^2); 3) IOD/BI-PH-5 C (1/

0.1 wt.) + 0.25 wt% of CNTs and monomers: DEGDA/DEGMA (1/1.5 wt%) (laser intensity: 200 mW/cm^2).

2.5.2. DLP 3D printing

3D objects evaluated in this study were printed via digital light processing DLP, using two DLP printer: 1) Zortrax Inkspire (from Zortrax, Poland) with averaged light output 2.72 mW/cm^2; 2) Anycubic Photon Mono (from Anycubic, China) with averaged light output 6.93 mW/cm^2. First, the CAD files of the designed models were created using Fusion360® software (from AutoDesk) and then the printing procedure was caried out at room temperature.

2.6. Nanocomposite resins

The following composition were prepared: BI-PH-5 C (0.2 wt%), IOD (2 wt%), DEGDMA/DEGDA monomers in a weight ratio of 1.5:1, and CNTs nanofillers, in weight amounts of: 0%, 0.1%, 0.25%, 0.5%, and 1.0%. The concentration of each component was calculated based on the monomers total weight. First, the Jacobs working curves were investigated followed by the photopolymerization kinetics and the effect of nanofiller concentration which were analyzed using a real-time FT-IR and photo-rheology. Finally, the 3D printing experiments were carried out using an Anycubic Photon Mono printer.

2.6.1. Jacob working curves

For the additive manufacturing of nanocomposite materials, Jacob working curves were created first in order to determine two key parameters: E_c (critical energy to initiate polymerization) and D_p (penetration depth of curing light) [61]. The relationship between curing intensity, curing time and curing depth can be expressed by a "working curve" as described by Jacob [62,63]. The values of these parameters are directly related to the type of resin, as its absorption, thus light penetration depth follows Lambert-Beer's law. Developing a Jacobs working curve has become the fundamental procedure for testing new resins when used in 3D printing [64,65], based on the Jacob's equation below:

$$C_d = D_p \ln\left[\frac{E_0}{E_c}\right] \tag{3}$$

where: C_d is the thickness of the cured resin, E_0 is the energy that was utilized to cure the resin, which is determined by the output of the printer and the curing time of the sample. E_c is the critical energy needed to start the photopolymerization (curing) process, and D_p is the depth of cure.

Using the Jacob working curve (C_d=f(E_0) as logarithmic), these two key parameters can be easily determined: E_c as the intersection of the graph with the X-axis and D_p as the slope of the curve.

2.6.2. Photo-rheological evaluation of nanocomposite photo-curing

Photo-rheological tests were performed using an Anton Paar Rheometer (Physica MCR 302) equipped with UV Light Curing System with a 20 mm parallel plates geometry (Fig. S127). As a source of light OmniCure® Series2000 lamp (product of Lumen Dynamics®, Canada) with bandpass filter to limit the wavelengths of light to 400 – 500 nm (part: P019–01047R) was applied, with light output set to 6.5 [mW•cm^{-2}] at the surface of the sample. The light intensity was measured by an PM160 - Si Sensor Power Meter (from Thorlabs Inc., Tampa, FL, USA). In the experiment, the distance between the two plates was set at 0.2 mm, with constant frequency of 10 Hz and strain amplitude of 1%. Light was turned on after 120 s after the start of the measurement in order to stabilize the system.

2.6.3. Characterization of 3D printed samples

2.6.3.1. Digital microscope. Digital microscope DSX1000 with an objective lens DSX10-SXLOB3X with a magnification of 42–420X (Olympus, Japan) was applied for the observation of 3D printouts.

2.6.3.2. Scanning electron microscope (SEM). For the imaging of 3D printouts morphology Mira3 XMU (Tescan, Czech Republic) was used. For the SEM investigation two samples were chosen: 1) hybrid printout – BI-PH-5B (0.1 wt%), IOD (1.0 wt%) and mixture of monomers: CADE/TMPTA (1/1 wt%); 2) nanocomposite printout – BI-PH-5C (0.2 wt%), IOD (2.0 wt%), CNTs (0.25 wt%) and mixture of monomers: DEGDA/DEGMA (1/1.5 wt%). Before the measurements the sample were coated with a 12 nm thin gold layer sputtered with ACE 600 coater (Leica, Germany) to ensure electric conductivity of the samples. The morphology of printouts was obtained at different magnifications in the resolution regime with the accelerating voltage of 10 kV using a standard Everhart-Thornley secondary electron (SE) detector and a low energy backscattered electron (BSE) detector.

3. Results

3.1. Spectroscopic properties

In order to fully characterize the spectroscopic properties of investigated biphenyl derivatives, the absorbance spectra, fluorescence quenching and fluorescence lifetime were measured and analyzed. The absorption properties of thee, newly discovered, group of biphenyl derivatives in acetonitrile: series A: 2-amino-4-methylbenzene-6-heteroaryl-1,3-dicarbonitriles; series B: 2-(diethylamino)– 4-methyl-6-heteroarylbenzene-1,3-dicarbonitriles; series C: 2-(diethylamino)– 4-(1-ethylpropyl)– 6-heteroarylbenzene-1,3-dicarbonitriles in acetonitrile are shown in Fig. 2, in the form of the molar extinction coefficient versus wavelength. All derivatives exhibit excellent absorption characteristics in the soft-UV and visible range, allowing the use of light from the safe visible range: LED @ 405 nm and even LED @ 415 nm.

Comparing the derivatives between the different series, it can be seen that changing the chromophore of these compounds directly affects the absorption characteristics: series A has the least extended spectrum towards longer wavelengths, thus these derivatives will be most effective using LED @ 405 nm and LED @ 365 nm light sources. However, the introduction of a diethylamine group at position two (B and C series) shifts the absorption bands of this groups towards longer wavelengths. In addition, the effect of substituents is noticeable, of which, as can be seen in Fig. 2, the proposed substituents do not significantly affect the absorption wavelength range, but the value of the molar extinction coefficient at specific wavelengths.

Table 1 contains spectroscopic data for the A, B, C series of the investigated biphenyl derivatives, with the molar extinction coefficient values determined at wavelengths corresponding to those of the light sources used in the kinetic studies.

3.2. Determination of usefulness of biphenyl derivatives as photosensitizers of iodonium salt for initiation of free-radical photopolymerization of acrylate monomer

The most popular type of photopolymerization are free radical polymerization processes, and they benefit from the wide range of monomers used in these reactions, including methacrylate and acrylate monomers. The major drawback of radical photopolymerization processes is the phenomenon of oxygen inhibition, which causes quenching of the excited states of the initiator by oxygen and consequently reduces the efficiency of the whole process. This type of polymerization is mainly initiated by radical initiators, but numerous scientific works have proven that the use of a dual-type initiating system based on a cationic initiator, e.g. iodonium salt, and an appropriate photosensitizer also effectively initiates radical photopolymerization processes. Therefore, the reported biphenyl derivatives together with iodonium salt (IOD) were proposed as an effective dual-type initiating system dedicated to

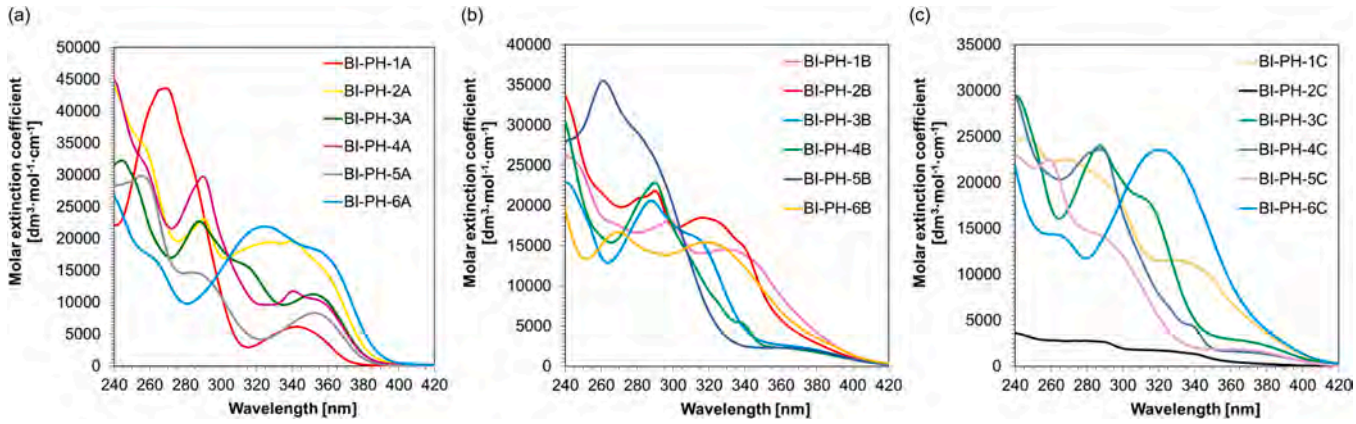

Fig. 2. UV–visible absorption spectra of a) series A - 2-amino-4-methylbenzene-6-heteroaryl-1,3-dicarbonitriles; b) series B - 2-(diethylamino)−4-methyl-6-heteroarylbenzene-1,3-dicarbonitriles; c) series C - 2-(diethylamino)−4-(1-ethylpropyl)−6-heteroarylbenzene-1,3-dicarbonitriles. Solvent: acetonitrile (ACN).

Table 1
Spectral characteristics of biphenyl derivatives studied in acetonitrile.

	Acronym	$\lambda_{max\text{-}ab}$* [nm]	$\varepsilon_{@\lambda max\text{-}ab}$* [$dm^3\ mol^{-1}\ cm^{-1}$]	$\varepsilon_{@405\ nm}$ [$dm^3\ mol^{-1}\ cm^{-1}$]	$\varepsilon_{@415\ nm}$ [$dm^3\ mol^{-1}\ cm^{-1}$]
Group A	BI-PH-1A	269	43.318	67	53
	BI-PH-2A	237	44.348	307	248
	BI-PH-3A	244	32.266	194	158
	BI-PH-4A	236	45.308	243	211
	BI-PH-5A	256	29.819	49	31
	BI-PH-6A	237	27.453	344	224
Group B	BI-PH-1B	205	31.079	887	391
	BI-PH-2B	214	35.075	699	311
	BI-PH-3B	213	32161	629	340
	BI-PH-4B	237	30.964	659	416
	BI-PH-5B	215	42.474	629	340
	BI-PH-6B	214	31.331	1022	405
Group C	BI-PH-1C	210	32.214	894	354
	BI-PH-2C	214	4.023	54	20
	BI-PH-3C	218	35.690	626	303
	BI-PH-4C	213	30.758	425	238
	BI-PH-5C	219	23.912	378	138
	BI-PH-6C	220	29.289	1054	483

*For the longest wavelength absorption band.

initiate the polymerization processes of acrylate monomer TMPTA. The initiating system was in the weight ratio: 0.1/1.0% - biphenyl derivative/IOD, and quantities were calculated relative to the monomer content. A mixture of: TMPTA and IOD (1.0%) was used as references. Conversion-time profiles for the two irradiation conditions under visible range: Vis-LED @405 nm are shown in Fig. 3, and under Vis-LED @415 nm are included in Supplementary Materials in Fig. S128.

As expected after the analysis of the absorption characteristics of these compounds, series A: 2-amino-4-methylbenzene-6-heteroaryl-1,3-dicarbonitriles turned out to be the weakest compared to the derivatives of series B and C - series A achieved similar conversion values upon illumination with 405 nm light, but the slope of the kinetic curve is by far the lowest for this group. However, all derivatives from this series except BI-PH-3A efficiently initiate photopolymerization processes at 405 nm, while the introduction of diethylamine group at position 2 in series B and C significantly improves the rate of the acrylate monomer polymerization process. When using light at 415 nm, the use of IOD/biphenyl derivative initiating systems at 1.0/0.1 wt% is inefficient, while their performance can be improved by increasing the concentration of the initiating system. In contrast, the derivatives from the B and C series perform excellently with the LED light source @415 nm, achieving acrylate conversion values up to 55%. When applying light at 405 nm, the performance of the Series B and C derivatives was similar, while differences in the performance of such systems can be seen clearly when using light at the 415 nm. 2-(diethylamino)−4-methyl-6-heteroarylbenzene-1,3-dicarbonitriles (Series B) proved to be most effective

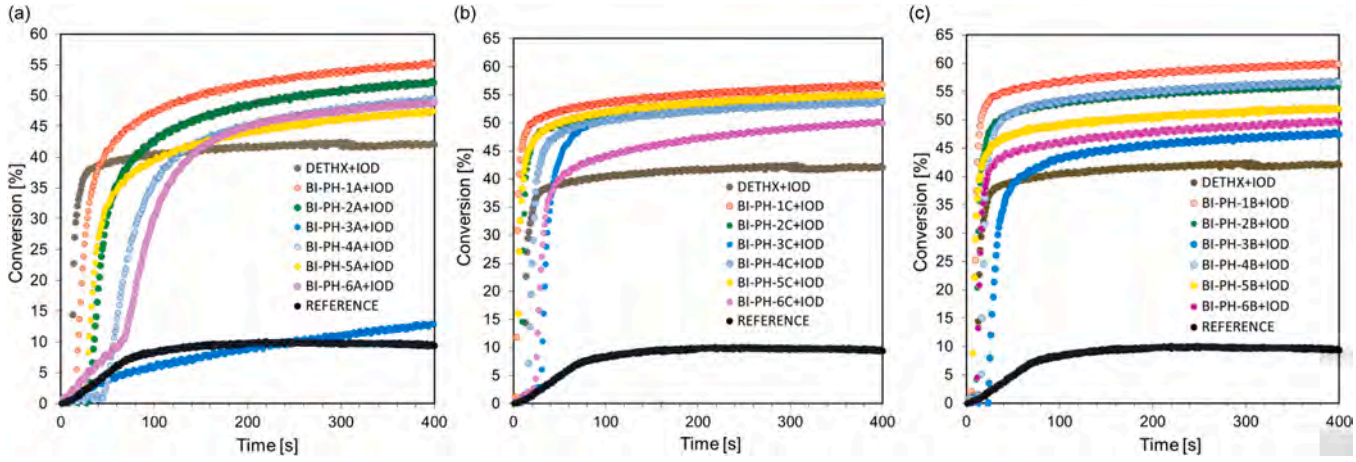

Fig. 3. Free-radical photopolymerization profiles (double bond conversion vs. time) for acrylate monomer and binary initiating system: IOD (1.0 wt%) and a) series A - 2-amino-4-methylbenzene-6-heteroaryl-1,3-dicarbonitriles (0.1 wt%); (b) series B - 2-(diethylamino)−4-methyl-6-heteroarylbenzene-1,3-dicarbonitriles (0.1 wt %), c) series C - 2-(diethylamino)−4-(1-ethylpropyl)−6-heteroarylbenzene-1,3-dicarbonitriles (0.1 wt%) under the irradiation at 405 nm.

with longer-wavelength light sources providing high reaction rates - high slope of the kinetic curve and relatively short induction times for these processes.

A summary of the conversion rates obtained for the acrylate monomer TMPTA under irradiation with Vis-LED @ 405 nm and Vis-LED @ 415 nm is shown in Table 2, and additional information regarding the slope of the kinetic curves and induction times can be found in Table S1 in Supplementary Information.

3.3. Determination of usefulness of biphenyl derivatives as photosensitizers of iodonium salt for initiation of cationic photopolymerization of epoxy monomer

The second type of photopolymerization is cationic polymerization, which is widely used due to its living nature, which makes it possible for the reaction to take place after the light source has been turned off. In addition, this type of reaction is resistant to oxygen, so that cationic polymerization reactions can be carried out "in the air." The effectiveness of a dual-type initiating system for the initiation of cationic polymerization of an epoxy monomer CADE was investigated. A composition consists of: BI-PH/IOD (0.1/1.0 wt%) and CADE monomer were investigated, and a mixture of CADE and IOD (1.0 wt%) was used as a reference. As in the case of radical photopolymerization, the ability of these systems to initiate the ring-opening cationic polymerization process was studied using two visible range light sources: Vis-LED @405 nm and Vis-LED @415 nm. Cationic photopolymerization profiles (oxirane ring opening conversion vs. time) for investigated cationic resins cured under LED @405 nm are shown in Fig. 4, and under LED @415 nm are presented in Fig. S129 in Supplement.

By analyzing the kinetic profiles of the cationic polymerization process, it is once again confirmed that the A-series is the least efficient, and some derivatives of 2-amino-4-methylbenzene-6-heteroaryl-1,3-dicarbonitriles do not initiate the ring-opening process at all, while some derivatives such as BI-PH-1A achieve significant degrees of epoxy monomer conversion. Excellent performance was shown by derivatives from groups B and C both under irradiation at 405 nm and 415 nm - significant conversion values were achieved with relatively high slopes of kinetic curves and short induction times.

A summary of the conversion rates obtained for the epoxy monomer CADE under irradiation with Vis-LED @405 nm and Vis-LED @415 nm is shown in Table 2, and additional information regarding the slope of the kinetic curves and induction times can be found in Table S1 in Supplementary Information.

Table 2
Summary of final functional group conversions of different monomers polymerized in various photopolymerization processes.

		Conversion [%]			
		Cationic polymerization CADE monitored at ~790 cm^{-1}		Free-radical polymerization TMPTA monitored at ~1635 cm^{-1}	
	Acronym	@ 405 nm	@ 415 nm	@ 405 nm	@ 415 nm
Group A	BI-PH-1A	85	24	55	47
	BI-PH-2A	94	57	52	np
	BI-PH-3A	np	np	13	22
	BI-PH-4A	np	np	49	37
	BI-PH-5A	83	55	47	6
	BI-PH-6A	np	np	49	13
Group B	BI-PH-1B	77	54	60	56
	BI-PH-2B	85	59	56	55
	BI-PH-3B	29	np	47	np
	BI-PH-4B	85	26	56	55
	BI-PH-5B	79	70	52	50
	BI-PH-6B	83	70	49	48
Group C	BI-PH-1C	83	77	57	53
	BI-PH-2C	85	69	54	54
	BI-PH-3C	np	np	55	45
	BI-PH-4C	75	33	54	57
	BI-PH-5C	84	77	55	54
	BI-PH-6C	67	58	50	58
Commercial reference (DETHX)		40	25	42	37

np – no polymerization.

3.4. Formation of interpenetrating polymer networks (IPN) at various conditions

As mentioned earlier, one of the limitations of radical polymerization of acrylate monomers is the phenomenon of oxygen inhibition. This effect can be limited by addition of a second monomer, acting e.g. according to the cationic mechanism, to form IPN, or Interpenetrating Polymer Network materials. Therefore, the biphenyl derivatives were examined for their performance during the simultaneous acrylate and epoxide photopolymerizations. One derivative from each series was selected, all having identical substituents: BI-PH-5A, BI-PH-5B, BI-PH-5C at 0.1 wt%, IOD (1.0 wt%), and a mixture of CADE/TMPTA monomers (1/1 wt.). To fully characterize the possibility of IPNs formation from the above compositions, the hybrid photopolymerization process was carried out in 3 different conditions: in laminate (between two polypropylene films - thin layer of 25 μm thickness), in air (on BaF_2 pallet - thin layer of 25 μm thickness), in air (in special attachment with BaF_2 - thick layer of 0.5 mm thickness) using LED light source @ 405 nm. Functional group conversions in IPNs formation are given in Fig. 5, and kinetic profiles for these photopolymerizations are shown in Figs. S130 in the Supplement.

The obtained values of conversion degrees of particular monomers undergoing hybrid polymerization clearly show that the proposed binary systems efficiently initiate the process of simultaneous cationic photopolymerization of epoxy monomer and free-radical polymerization of acrylate monomer. Different final degrees of monomers conversion were obtained depending on the process conditions. It can be noticed, however, that the addition of epoxy monomer to acrylate monomer effectively improves the efficiency of acrylate polymerization under conditions when the sample is exposed to oxygen - it allows to decrease the negative effect of oxygen inhibition. A summary of the conversion degrees obtained is shown in Table 3.

3.5. Free-radical photopolymerization with biphenyl/MDEA as type II initiating system

As confirmed later by electrochemical studies and thermodynamic calculations, the reported derivatives exhibit not only photo-oxidative properties, allowing their use as sensitizers of iodonium salt in the photo-oxidation cycle, but also show photo-reducing properties, thus allowing their use together with the co-initiator (amine) in initiation processes according to the photo-reduction mechanism. Type II radical photoinitiators generate radicals in the presence of a co-initiator in a multistep process in which an excited molecule of a biphenyl derivative interacts with an electron donor (amine - co-initiator) and becomes an electron acceptor. An example of such a co-initiator can be methyl diethanolamine – MDEA. Therefore, the analyzed derivatives were tested for their applicability in II-type initiator systems. For this purpose, the performance of biphenyl derivatives in three types of compositions was compared: 1) BI-PH-3A or BI-PH-3B or BI-PH-3 C (0.1 wt%) + MDEA (1.5 wt%) + TMPTA; 2) BI-PH-3A or BI-PH-3B or BI-PH-3 C (0.1 wt%) + IOD (1.0 wt%) + TMPTA; 3) BI-PH-3A or BI-PH-3B or BI-PH-3 C (0.1 wt%) + MDEA (1.5 wt%) + IOD (1.0 wt%) + TMPTA. Measurements were conducted in the laminate (between two polypropylene films), using an LED light source @ 405 nm. Free-radical photopolymerization profiles for TMPTA with above mentioned initiating systems are presented in Fig. 6.

The analyzed derivatives are able to initiate radical polymerization processes both according to the photo-oxidation mechanism with

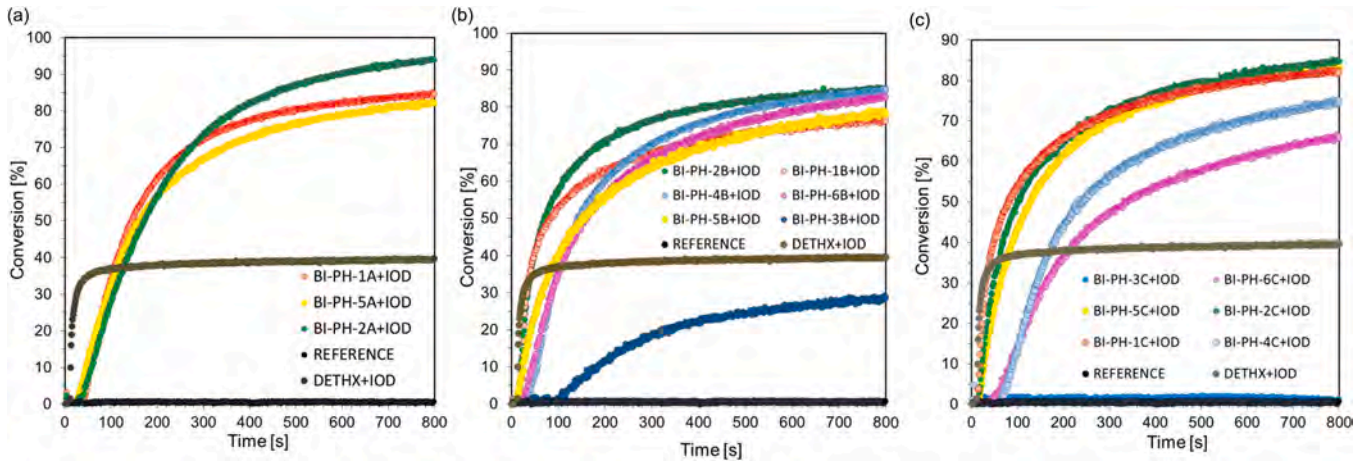

Fig. 4. Cationic photopolymerization profiles (oxirane ring opening conversion vs. time) for epoxy monomer and binary initiating system: IOD (1.0 wt%) and (a series A - 2-amino-4-methylbenzene-6-heteroaryl-1,3-dicarbonitriles (0.1 wt%); (b) series B - 2-(diethylamino)−4-methyl-6-heteroarylbenzene-1,3-dicarbonitriles (0.1 wt%), c) series C - 2-(diethylamino)−4-(1-ethylpropyl)−6-heteroarylbenzene-1,3-dicarbonitriles (0.1 wt%) under the irradiation at 405 nm.

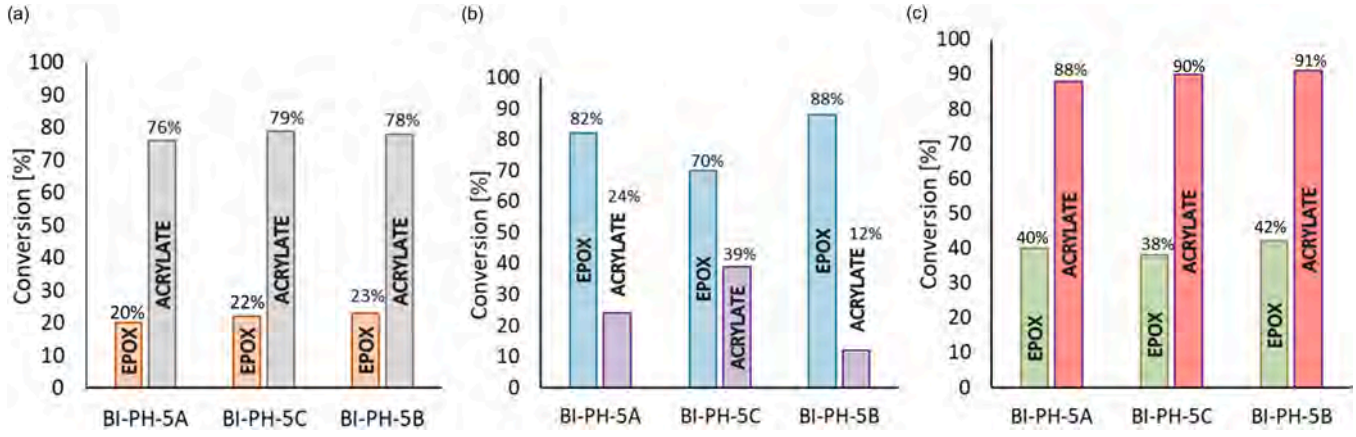

Fig. 5. Values of conversion obtains during hybrid CADE/TMPTA (50/50 wt%) photopolymerization at different conditions: a) in laminate (between two polypropylene films), sample thickness 25 μm.; b) in the air (on BaF_2 pallet), sample thickness 25 μm; c) in the air (thick layer), sample thickness 0.5 mm; with the use of biphenyl derivatives (0.1 wt%) and iodonium salt (1.0 wt%) under the irradiation at 405 nm.

Table 3
Functional group conversions obtained in the process of photo-formation of various types of IPN networks, using photoinitiating systems based on IOD (1 wt %) and representatives of biphenyl derivatives of each series (0.1 wt%), determined by real-time FT-IR.

Exposure to LED light at @405 nm					
Composition	**Experimental conditions and monitoring wavelengths**		**Functional group conversion**		
			BI-PH-5A	**BI-PH-5B**	**BI-PH-5 C**
CADE/TMPTA (1/1 w/w)	Laminate	EPOX at 790 cm^{-1}	20	23	22
		ACRYLATE at 1635 cm^{-1}	76	77	70
	Air thin layer	EPOX at 790 cm^{-1}	82	88	79
		ACRYLATE at 1635 cm^{-1}	24	12	39
	Air thick layer	EPOX at 3700 cm^{-1}	40	42	38
		ACRYLATE at 6165 cm^{-1}	88	90	90

iodonium salt (IOD) and according to the photo-reduction process with amine (MDEA), however, the obtained conversion rates are not completely satisfactory. Therefore, the performance of biphenyl derivatives in the three-component initiation systems: biphenyl-iodonium salt-amine, was verified to determine their applicability in the reversible photo-oxidation cycle. As can be seen in Fig. 5, such ternary systems are the most effective while providing: high conversion rates, short induction times, and a significant rate of photopolymerization of the acrylate monomer TMPTA.

3.6. Analysis of photoinduced electron transfer process with photo-oxidation and photoreduction mechanism between iodonium salt and investigated biphenyl derivatives

In order to determine the suitability of the proposed derivatives in two-component initiating systems operating according to a photo-oxidation or photo-reduction mechanism, electrochemical tests were carried out to determine the oxidation and reduction potentials of these compounds and calculations were performed to establish the thermodynamic parameters of the analyzed systems.

First, the performance of binary biphenyl derivative/iodonium salt initiating systems in photo-oxidation was analyzed. In such a system, the biphenyl derivatives initiate an electron transfer process between their excited state and the iodonium salt molecule. In this process, the

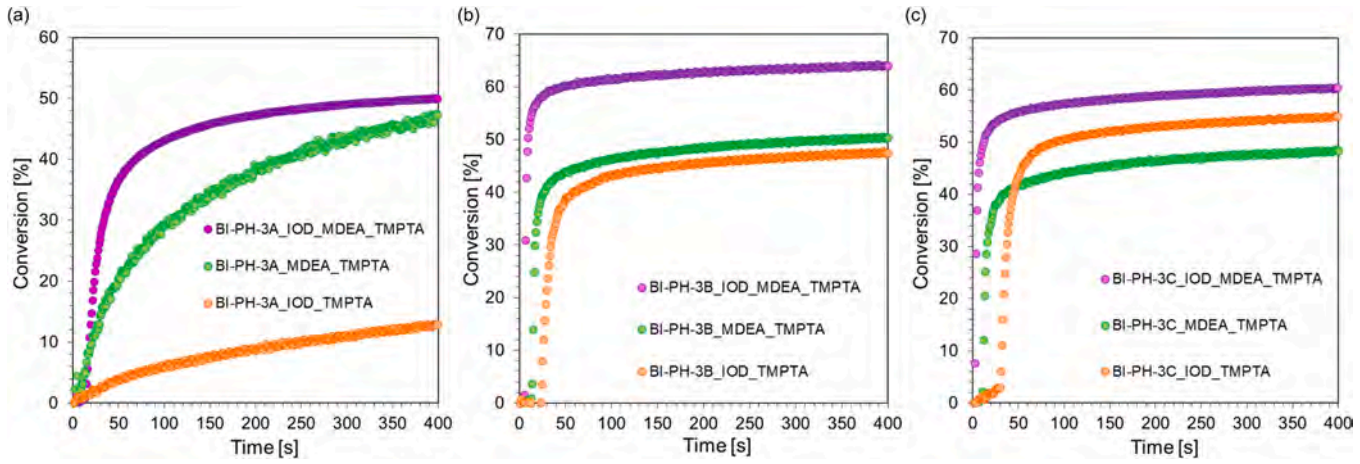

Fig. 6. Free-radical photopolymerization profiles (acrylate function conversion vs. irradiation time) for TMPTA with different initiating system (IOD (1.0 wt%), MDEA (1.5 wt%) or IOD/EDB (1.0/ 1.5 wt%) and appropriate derivative: (a) BI-PH-3A; (b) BI-PH-3B; (c) BI-PH-3C, during the exposure to LED light at @ 405 nm.

biphenyls act as photosensitizers and upon absorption of light become electron donors for the iodonium salt, which as an electron acceptor is reduced in this process. On the basis of oxidation and reduction potentials of individual components, Gibbs' free energy ($\Delta G_{et(S1)}$) was determined by applying the classical Rehm-Weller equation. All analyzed biphenyl derivatives of A, B and C series exhibit sufficiently low oxidation potentials to participate effectively in the electron transfer process together with the iodonium salt and thus to initiate the photopolymerization process according to this mechanism - the value of $\Delta G_{et\ (S1)}$ is negative.

In addition, to confirm the electron transfer mechanism between the biphenyl derivative and the iodonium salt fluorescence quenching experiments were carried out by analyzing the change in emission intensity of the biphenyl derivatives in acetonitrile as the iodonium salt was added to the solution. A linear relationship was observed between the emission intensity of the derivatives and the concentration of initiator present in the system. On this basis, the Stern-Volmer coefficients (K_{SV}) (Equation S1) were determined and the reaction constant (k_q) (Equation S2) between the diaryliodonium salt and the excited singlet state of the biphenyl compound in the photo-oxidation mechanism was calculated. Finally, the quantum yield of electron transfer from the excited singlet state ($\Phi_{et\ (S1)}$) in the photo-oxidation process (Equation S3) was determined. The obtained values are summarized in Table 4 and the derivation of the equations are included in the Supplementary Information along with voltammetry curves of cyclic oxidation of biphenyl derivatives, fluorescence lifetime decay results and fluorescence quenching results of the studied compounds.

As it has been pointed out in experimental studies, the analyzed biphenyl derivatives are also able to initiate polymerization according to the photo-reduction mechanism. In this type of process, the excited photosensitizer molecule is the electron acceptor, and the role of the donor is taken by the so-called co-initiator, which can be an amine (MDEA). From the reduction potentials of biphenyl derivatives and the oxidation potential of methyl diethanolamine, Gibbs' free energy (ΔG_{et}

Table 4
Electrochemical and thermodynamic properties of series A, B and C of biphenyl derivatives in the photo-oxidation mechanism.

	Acronym	$E_{ox\ vs\ Ag/AgCl}$ [mV]	E_{S1} [eV]	$\Delta G_{et\ (S1)}$ [a)] [eV]	$\tau_{(S1)}$ [ns]	K_{sv} [M^{-1}]	k_q [$M^{-1}s^{-1}$]	$\Phi_{et\ (S1)}$
Group A	BI-PH-1A	1291	3.02	–1.09	3.01	167.6	$5.57{\cdot}10^{10}$	0.78
	BI-PH-2A	1311	3.10	–1.15	4.30	121.7	$2.83{\cdot}10^{10}$	0.72
	BI-PH-3A	1783	2.32	–0.81	3.12	40.5	$1.30{\cdot}10^{10}$	0.46
	BI-PH-4A	1363	3.24	–1.23	3.68	25.6	$6.97{\cdot}10^{9}$	0.35
	BI-PH-5A	1273	3.00	–1.08	nc	7.0	nc	nc
	BI-PH-6A	1531	3.17	–1.00	2.43	65.9	$2.71{\cdot}10^{10}$	0.58
Group B	BI-PH-1B	1307	2.99	–1.04	2.36	76.4	$3.24{\cdot}10^{10}$	0.62
	BI-PH-2B	1327	3.00	–1.03	2.63	267.4	$1.02{\cdot}10^{11}$	0.85
	BI-PH-3B	1551	3.00	–0.80	2.35	8.9	$3.77{\cdot}10^{9}$	0.16
	BI-PH-4B	1351	3.01	–1.02	3.25	40.5	$1.25{\cdot}10^{10}$	0.46
	BI-PH-5B	1309	3.24	–1.29	2.65	16.1	$6.30{\cdot}10^{9}$	0.23
	BI-PH-6B	1539	3.00	–0.82	2.67	602.7	$2.26{\cdot}10^{11}$	0.93
Group C	BI-PH-1C	1301	3.24	–1.30	2.23	6.9	$3.08{\cdot}10^{9}$	0.13
	BI-PH-2C	1323	3.21	–1.25	2.34	108.0	$4.35{\cdot}10^{11}$	0.96
	BI-PH-3C	1557	3.09	–0.90	2.41	40.5	$1.68{\cdot}10^{10}$	0.46
	BI-PH-4C	1331	3.16	–1.18	3.14	40.5	$1.29{\cdot}10^{10}$	0.46
	BI-PH-5C	1254	2.99	–1.09	2.57	40.5	$1.58{\cdot}10^{10}$	0.46
	BI-PH-6C	1538	2.97	–0.80	2.68	19.9	$7.41{\cdot}10^{9}$	0.29

[a] calculated from the classical Rehm-Weller equation:

$$\Delta G_{et} = F[E_{ox}(D/D^{\bullet+}) - E_{red}(A^{\bullet-}/A)] - E_{00} - \left(\frac{N_A e^2}{4\pi\varepsilon_0\varepsilon_r a}\right)$$

Eox ($D/D^{\cdot+}$) – electrochemically determined oxidation potential of the electron donor
Ered ($A^{\cdot-}/A$) – electrochemically determined reduction potential of the electron acceptor (– 0.64 V for the diphenyliodonium salt vs. Ag/AgCl) [66,67]
E_{S1} – singlet state energy of the sensitizer determined based on excitation and emission spectra (Figs. S55-S72 in Supplementary)
Φ_{et} – quantum yield of electron transfer (Equation S3)
$\Phi_{et} = K_{SV}[IOD]/(1 + K_{SV}[IOD])$ for the concentration of iodonium salt [IOD] 0.021 mol/dm^3
nc – not calculated

$_{(S1)}$) was calculated for the type II initiating system. The obtained values, experimental and calculated, are summarized in Table S2. Most of the biphenyl derivatives have sufficiently low reduction reduction potentials to react efficiently with the amine in the type-II initiating binary system - as confirmed by the negative $\Delta G_{et(S1)}$ values.

3.7. Investigation of printing performance of various resin containing the developed two component initiating system: biphenyl derivative/iodionium salt

3.7.1. Laser 3D Printing

A representative biphenyl derivative, BI-PH-5B (0.1 wt%), an iodonium salt (1.0 wt%) and a 1:1 mixture of acrylate (TMPTA) and epoxy (CADE) monomers were selected for the laser 3D printing experiments. The resulting 3D printout exhibited a significant height with excellent optical resolution (Fig. 7, top raw). Fig. 7, down raw, displays SEM micrographs of the printed material, the "D" element, showing the morphology and defects not visible by the optical microscopy. The SEM analysis detected a presence of unknown elements in the structure of the D element. The geometry and size of the element together with the contrast on the BSE detector likely caused by the high atomic mass of Iodonium atoms (Fig. 7, bottom right image) allows us to conclude that crystals of undissolved iodonium salt were present in the printed material, which was previously unnoticed. This analysis allows us to further improve the composition for 3D printing resins in order to obtain homogeneous printouts with the desired final parameters.

3.7.2. Digital light processing (DLP) printing

A derivative with the acronym BI-PH-5 C was selected for the 3D printing experiments using the digital light processing (DLP). It was used as part of a ternary initiator system (0.2 wt%) along with IOD iodonium salt (2.0 wt%) and MDEA amine (3 wt%). The resin base was a mixture of monomers: 2-hydroxyethyl methacrylate (HEMA) and bisphenol A ethoxylate diacrylate (BEDA) in a mass ratio of 3:7. This system was used to print a 10×10×10 mm 3D model cube using a DLP printer - Zortrax Inkspire. Photographs of the printout obtained using an optical microscope, with sectioning and detailed analysis of the printout are included in Fig. 8.

As shown in Fig. 8, the resulting printout has high optical resolution using only two simple methacrylate and acrylate monomers HEMA/BEDA and a ternary initiator system: BI-PH-5 C/IOD/MDEA (0.2/2.0/3.0 wt%). In addition, the kinetic profile for the photopolymerization process of the composition used for the above printing can be found in Supplementary Information in Fig. S132.

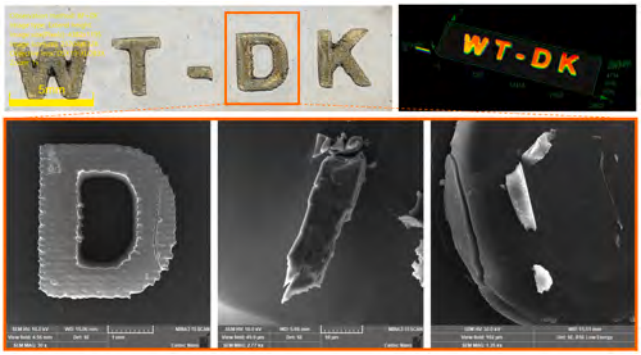

Fig. 7. 3D printouts obtained by exposing to laser source of light composition BI-PH-5B (0.1 wt%) + IOD (1.0 wt%) + mixture of monomers: CADE/TMPTMA (1/1 wt.). The top row contains images obtained from an optical microscope, while the bottom row contains images of the morphology of the "D" element of the printout, obtained using SEM (the scale bar represents left: 1 mm; middle and right: 10 μm) from SE (left and middle) and BSE (right) signal.

3.8. Manufacturing of CNTs composites

Last, but not least, our goal was to test whether the initiation systems containing the reported biphenyl derivatives could be used to initiate photopolymerization processes in the presence of a nanofiller. Carbon nanomaterials such as carbon nanotubes (CNTs), carbon black (CB), or graphene represent a common additive used with various polymer matrices to introduce electric conductivity and enhance their thermo-mechanical properties and thermal conductivity [68,69]. In combination with printing techniques, it allows a rapid design and fabrication of various electronic parts and devices such as sensors, Joule heaters or flexible electronics [70,71]. Nevertheless, the VAT 3D printing techniques suffers from the adverse effects of increased viscosity and reduced photo-curing conversion, especially at higher filler content. Mu, et al. established an optimal CNT concentration in a commercial photo-curable resin to 0.3 wt% above which the formulations lose a good printability by a DLP printer [72]. Analogically, Gonzalez, et al. reported a drop in curing efficiency by 50% upon the addition of 1 wt% of CNTs to a mixture of poly(-ethylene glycol) diacrylate (PEGDA) and poly(ethylene glycol) methyl ether methacrylate (PEGMEMA) monomers with 3 wt% of the standard commercial photoinitiator bis(2,4,6-trimethylbenzoyl)-phosphineoxide (BAPO) [56]. Moreover, the conversion rate was not fully restored even after doubling the photoinitiator concentration to 6 wt% and a reactive solvent diluent had to be added to achieve a good printability.

We, on the other hand, demonstrate a different approach in improving the printability of high-concentration photocurable nanocomposites by the application of high-efficiency photoinitiating systems. Multiwalled carbon nanotubes (MWCNTs) were used as the nanometric filler to the mixture of the monomers containing di(ethylene glycol) dimethacrylate (DEGDMA), and di(ethylene glycol) diacrylate (DEGDA), which are reported in the literature to be suitable for the appropriate dispersion of carbon nanotubes [56]. It is a well-established fact that the quality of nanoparticle dispersion in a liquid medium is closely related to the balance of physico-chemical forces [49,50]. Undesired macroscale aggregation would lead to a sedimentation and uneven distribution of the CNTs through the printed body.

3.8.1. Characterization of nanocomposites' fabrication process based on photopolymerization

The photopolymerization kinetics and the effect of the CNTs content on the photopolymerization were analyzed using the real-time FT-IR technique. The samples with CNTs content ranging from 0% to 1.0% were examined in air, in the ring form, sample dimension: 1.5 mm thickness and 12 mm diameter. Free-radical photopolymerization profiles (double bond conversion vs. time) for nanoresins are shown in Fig. 9a, the dependence of the slope of the kinetic curves on the nanotube content is shown in Fig. 9b and the FT-IR spectra before and after photopolymerization process are presented in Supplementary Information (Figs. S133-S137). The obtained results clearly show that the photopolymerization reaction slows down as the CNT content increases which is manifested by the decreasing slope of the conversion curves. Nevertheless, all samples eventually achieved the final conversion of 95–100% regardless of the CNT content. Hence, these new compounds can shift the boundaries of printable materials to higher CNT loadings and/or higher viscosities of the photocurable resins or reduce the printing times of the existing formulations.

Photo-rheological experiments were performed to investigate the effect of the nanofiller on the curing time as well as on the rheological properties of the resin itself. The time dependence of the storage modulus (G′) through the photopolymerization for resins with CNT content ranging from 0% to 1.0%, where the sample without CNTs (0.0 wt%) is treated as a reference, is shown in Fig. 10a. A pronounced effect of the CNT content on the rheological properties was evident. As the amount of CNTs increased, the storage modulus (G′) took on higher values.

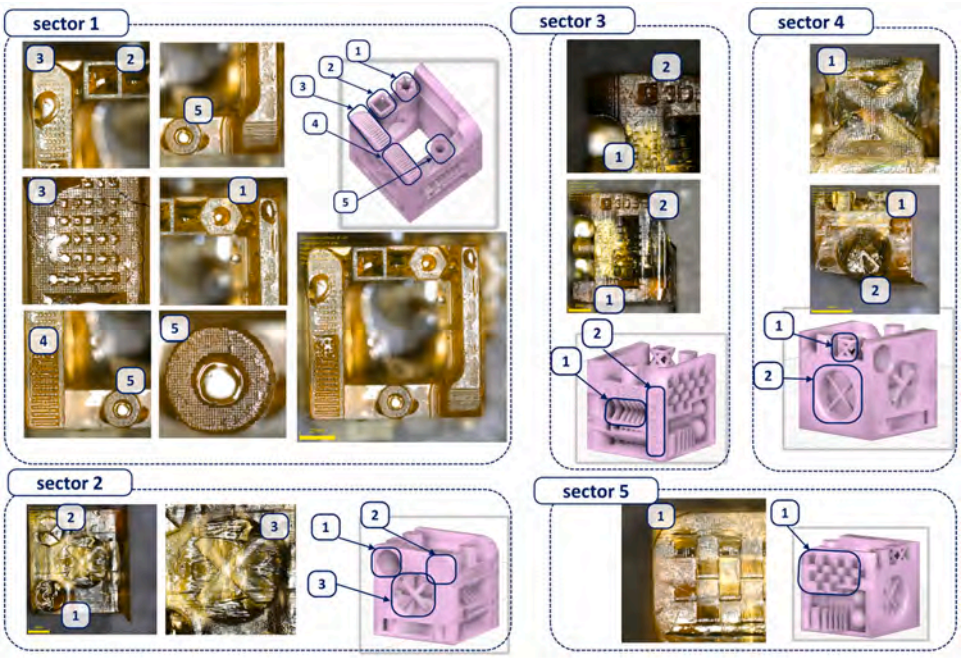

Fig. 8. Model 3D cube printout with dimensions of 10×10×10 mm using DLP printer - Zortrax Inkspire. Description: SECTOR 1: 1 - hexagon with circular inner cutout - correct object geometry and sharp edges characterize a well-chosen initiating system.; 2 - grid - general test, which determines overall performance of 3D system; ideal test: an object composed of thin trusses is created; 3 - system capability test in X and Y axis (indentation) - printing cylindrical parts with variable size from 0.05 mm to 0.20 mm. The test reveals the real optical resolution of the system in X and Y axes; 4 - test of system capabilities in X and Y axes (projections) - printing cylindrical elements of variable size from 0.05 mm to 0.20 mm. The test reveals the true optical resolution of the system in X and Y axes; 5 - cylinder - correct object geometry and edge sharpness characterizes a well-chosen initiator system. SECTOR 2: 1 - minimum wall thickness test – contains a spherical hollow. The test evaluates the effectiveness of the entire 3D system and states about its efficiency; 2 - indentation with increasing depth from 0.025 mm to 0.020 mm; 3 - calibration test: multidirectional symmetrical ridges are placed in a circular cut-outs. The test shows possible problems with overexposure or excessive optical transparency of the polymer - all elements should be clear and symmetrical. SECTOR 3: 1 - the test determines the focusing quality and resin characteristics. Blurred elements indicate that the resin polymerizes outside the exposed elements; 2 - text: the test contains "3D" text. The text is visible to the bare eye and indicates a good fit between the resin and the printer. The test allows to estimate the depth of polymerization: if the text is visible and sharp it means that the exposure time was chosen correctly. SECTOR 4: 1 - general purpose test which determines overall performance of 3D system; ideal test: an object consisting of thin trusses is created; 2 - thin cross-shaped bridges of 0.5 mm in diameter crossing the center of a circular cut-out - evaluates the suitability of the resin for printing. SECTOR 5: 1 - checkerboard: square cuts of 1 × 1 mm in size and 0.75 mm deep form a checkerboard pattern. This is the most important test to determine the overall performance of the resin.

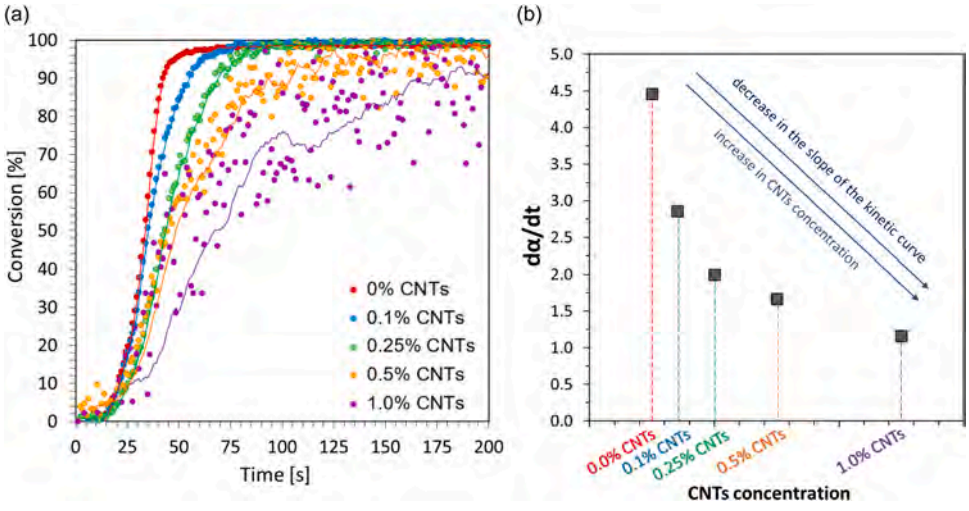

Fig. 9. (a) Free-radical photopolymerization profiles (double bond conversion vs. time) for a mixture of monomers: DEGDA/DEGMA (1/1.5 wt%) and binary initiating system: IOD (2.0 wt%) and (a) BI-PH-5 C (0.2 wt.) and different amount of MWCNTs (0; 0.1; 0.25; 0.5; 1.0 wt%). Experiment conditions: in the air in the ring sample thickness: 1.5 mm. Irradiation source: LED at 405 nm. (b) Slope of the kinetic curves vs CNTs concentrations.

The crossover of the storage (G′) and loss moduli (G"), which indicates the gelation point for the curing process of the studied nanoresins, was only detectable in the reference sample with no CNTs. That was possible because its initial storage modulus (i.e., prior the photocuring) was lower than its initial loss modulus (Fig. 10b). Both moduli grow as the curing proceeds (Fig. 10b) but the increase in storage modulus is much more pronounced as the growing polymer network percolates through the whole volume of the sample. This is accompanied by a noticeable change in rheologic properties – the gel point. However, the addition of even a low amount of CNTs caused the initial storage modulus to exceed the loss modulus (Figs. S138-S141) due to the formation of a physical network which is capable to bear a load. Noteworthy, the rheological properties are very sensitive to the nanoparticle arrangement but only brings an indirect evidence of the inner structure [73]. The initial storage modulus increased from about 1 mPa for the reference sample to approx. 2 kPa for the sample containing 1.0% CNTs,

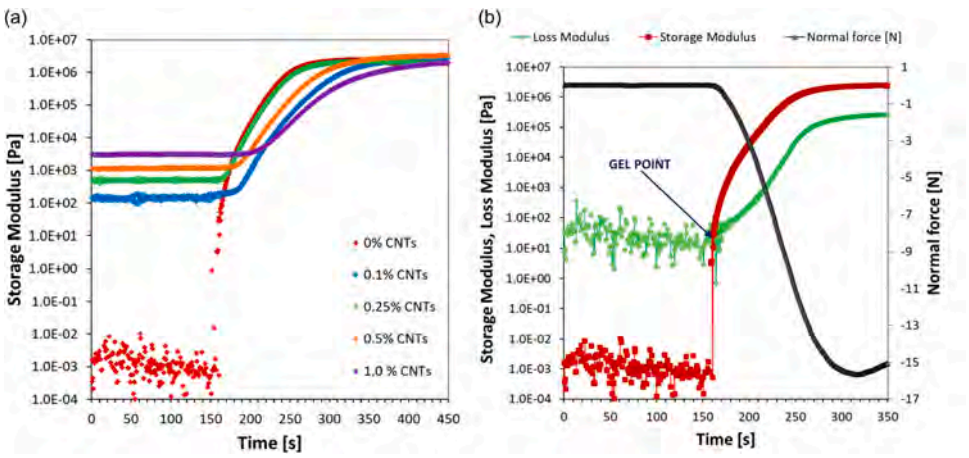

Fig. 10. a) Storage modulus. G′ versus irradiation time for DEGDA/DEGMA (1/1.5 wt%) formulations containing CNTs with concentration ranging from 0 wt% up to 1.0 wt%. Film thickness 100 μm. irradiation power 5.6 mW/cm^2 (405 nm); b) The storage (red) and loss modulus (green) as well as normal force (black) as a function of the irradiation time for SPOT LV sample: BI-PH-5 C (0.2 wt%), IOD (2.0 wt%) and DEGDA/DEGMA (1/1.5 wt%), without CNTs.

that is by more than 6 orders of the magnitude. This increase matched well with similar results reported in the literature [72]. Such phenomenon is commonly observed for nanoparticles with high aspect ratio such as CNTs, unless they are too aggregated, and is accompanied with a large increase in the initial viscosity which could be considered as an adverse effect for the 3D printing. Nevertheless, all the samples exhibited a further increase of the storage modulus upon the curing with no significant variation in the final value (Fig. 10a).

With the kinetics of photopolymerization process studied and the effect of nanofiller content on the curing process analyzed, we attempted to 3D print from the investigated compositions. For this purpose, the sample: BI-PH-5 C (0.2 wt%), IOD (2.0 wt%), CNTs (0.25 wt%) and DEGDA/DEGMA (1/1.5 wt%) was chosen. The first experiment was laser engraver printing, in order to prove that the tested composition is suitable for the 3D-VAT process. The letter "A" was printed, and its morphology was analyzed using SEM. Analysis of the printed structure showed a presence of agglomerated CNTs in the cured resin (Fig. 11), which will compromise the printing properties of the nano-resin.

Therefore, the nanoresin was subjected to additional sonification with a SONOPULS ultrasonic homogenizer (from Berlin, Germany) before testing on a DLP printer, which allowed much better dispersion of the nanofiller. Prior to the final printing, key parameters for the 3D-VAT printing process were determined: E_c (critical energy to initiate polymerization) and D_p (penetration depth of curing light) [61]. To determine E_c and D_p, thin slices with design dimensions of 1×1x 0.3 mm were printed, and the sample exposure time was varied: 120 s, 110 s, 90 s, 70 s, 50 s, with a constant light output of 6.93 mW/cm^2. The printing thickness (C_d) was then measured using a micrometer screw gauge, and the thickness measurements were repeated 5 times for each sample. The dependence of print thickness on E_0 - energy that was utilized to cure the resin, as well as images of the printed slicer are shown in Fig. 12a.

Using the Jacob working curve (C_d=f(E_0) as logarithmic), these two key parameters was easily determined: E_c as the intersection of the graph with the X-axis (56 mJ/cm^2) and D_p as the slope of the curve (95 μm). From the obtained data, the minimum time needed to cure the thin layer was determined to be 8 s, so the first approach was to print an example 3D model with a time slightly above the critical time: 10 s. Using such a short curing time for the layer, a printout with a final thickness of 100 μm was obtained, as seen in Fig. 12a.

Having all the necessary information on the photopolymerization process in the presence of nanofiller and having determined E_c and D_p values, we attempted to print the final object using a light exposure time of 35 s and a thickness of one layer of 100 μm. Photographs of the final printout are shown in Fig. 13.

4. Conclusions

In this paper, it has been shown how significant role is played by the photoinitiating system in additive manufacturing processes, specifically involving 3D-VAT printing. Three groups of the biphenyl derivatives differing in the type of chromophore as well as in the type of substituent were newly synthetized. A detailed spectroscopic, electrochemical and thermodynamic analysis of these derivatives was presented alongside to the possibility of their use in two-component photoinitiating systems, operating according to a photo-oxidation mechanism (with an iodonium salt) or a photo-reduction mechanism (with an amine). The performance

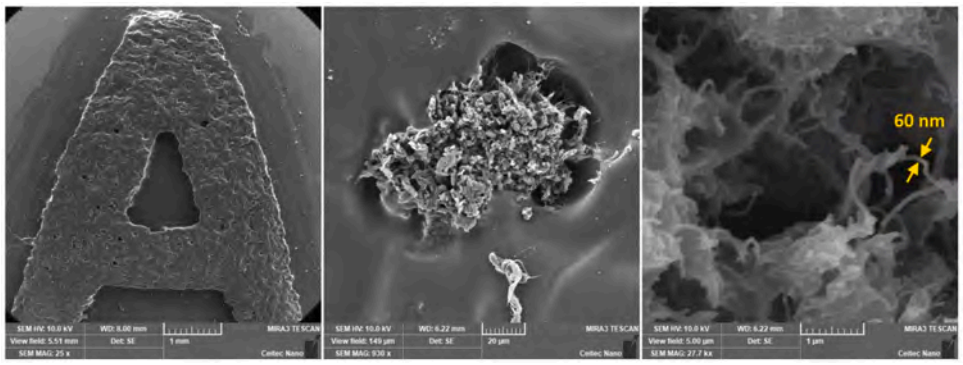

Fig. 11. SEM images of 3D printed nanocomposites (letter A) obtained from composition BI-PH-5 C (0.2 wt%), IOD (2.0 wt%), CNTs (0.25 wt%) and DEGDA/DEGMA (1/1.5 wt%) via laser engraver (source of light – LED @405 nm). The scale bar represents 1 mm (left); 20 μm; and 1 μm (right).

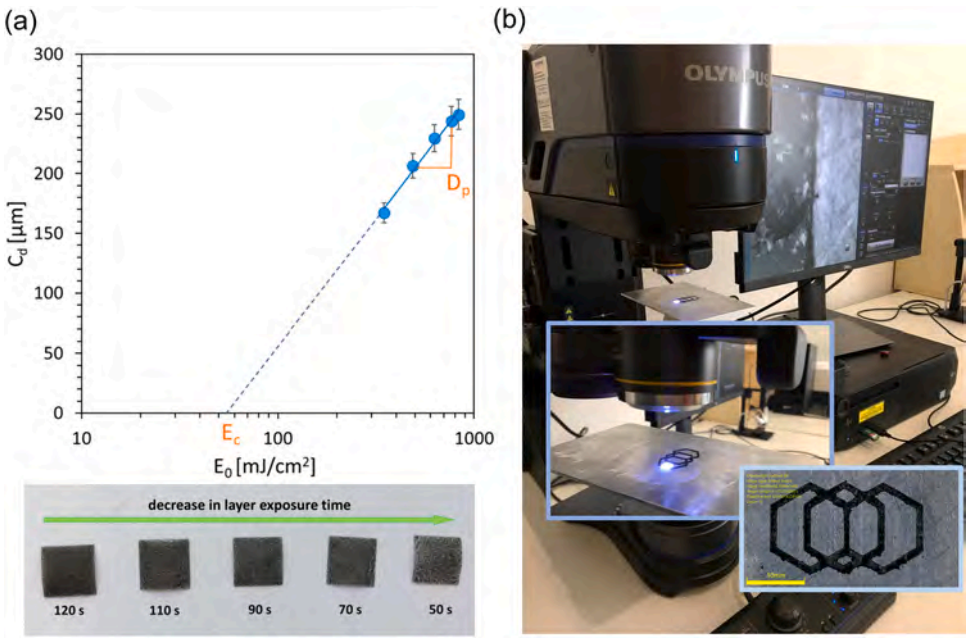

Fig. 12. (a) Jacob working curves for composition: BI-PH-5 C (0.2 wt%), IOD (2.0 wt%), CNTs (0.25 wt%) and DEGDA/DEGMA (1/1.5 wt%) exposed to 405 nm light (6.93 mW/cm^2); (b) Photograph of the final printout obtained using the minimum light exposure time of the sample and an image of material acquired by optical microscopy.

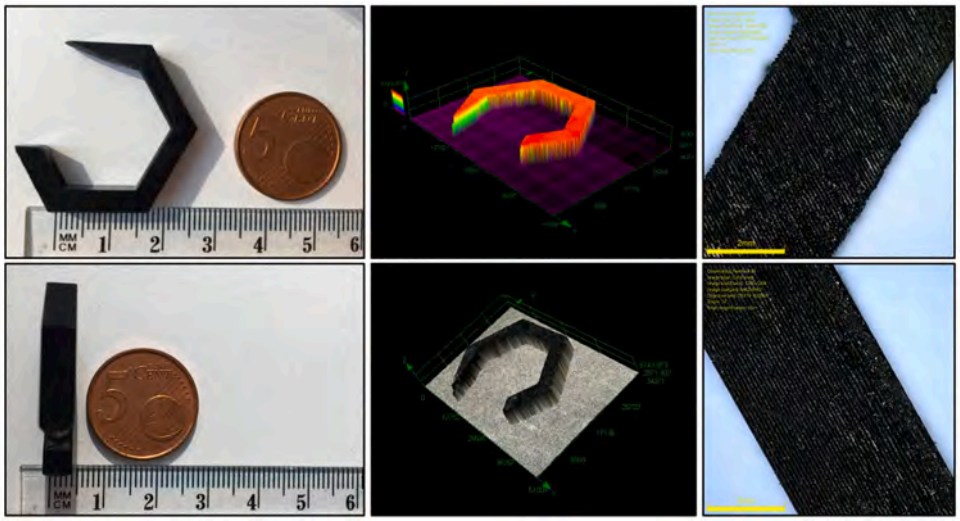

Fig. 13. Images of final 3D printout obtained via DLP printing, using nanoresin consisted of: BI-PH-5 C (0.2 wt%), IOD (2.0 wt%), CNTs (0.25 wt%) and DEGDA/DEGMA (1/1.5 wt%), light source: LED, 405 nm (6.93 mW/cm2). Printing accuracy in the X-, Y- and Z- directions: ± 0.03 mm.

of these derivatives in initiating various polymerization reactions including a free-radical photopolymerization of acrylate monomer TMPTA, a cationic ring-opening photopolymerization of epoxy monomer CADE, and a hybrid photopolymerization of CADE/TMPTA monomers was compared. From these studies, it was concluded that the introduction of a diethylamine group into the position two of the chromophore improves the sensitizing properties of the derivatives.

The most effective compound was tested as a photosensitizer in light-initiated polymerization in a two-component photoinitiating system dedicated to photosensitive polymer resins for 3D printing, including nanoresins filled with carbon nanotubes. The effect of the nanofiller on the kinetics of the photopolymerization process was analyzed using real-time FT-IR and photo-rheology, which was crucial for improved selection of the resin composition and optimization of the printing parameters itself. In addition, key printing parameters were determined, i.e. E_c (critical energy to initiate polymerization) and D_p (penetration depth of curing light). We have demonstrated the feasibility photosensitive resins containing bipfenyl–iodonium salt initiating system, of printing CNTs nanocomposite materials of significant dimensions using digital light processing-based printing (DLP), and we have characterized the finished printouts using optical microscopy and scanning electron microscopy. These results are a promising start for the search for resins/nanoresins with appropriate initiating system, to fabricate multimaterials using advanced additive techniques, specifically 3D VAT printing, such as DLP or SLA.

Declaration of Competing Interest

The authors declare that they have no known competing financial interests or personal relationships that could have appeared to influence

the work reported in this paper.

Acknowledgements

This research was funded by the Foundation for Polish Science (Warsaw, Poland) TEAM TECH project Grant No. TEAM TECH/2016–2/15 (POIR.04.04.00–00-204B/16–00).

Moreover, the Polish group acknowledge the support of the PROM programme for the financing of the international internship for PhD student (W.T.) no. PPI/PRO/2019/1/00018, which is co-financed by the European Social Fund under the Knowledge Education Development Operational Programme.

We also acknowledge the CzechNanoLab Research Infrastructure supported by MEYS CR (LM2018110) for providing the equipment for SEM analysis.

Appendix A. Supporting information

Supplementary data associated with this article can be found in the online version at doi:10.1016/j.addma.2021.102447.

References

[1] A. Polykarpov, Tiwari Tiwari, Photocured Materials, in: A. Polykarpov, A. Tiwari (Eds.), Photocured materials: A general perspective, 1st ed.,, Royal Society of Chemistry, Cambridge, 2015, pp. 1–14.
[2] I. Kamińska, J. Ortyl, R. Popielarz, Mechanism of interaction of coumarin-based fluorescent molecular probes with polymerizing medium during free radical polymerization of a monomer, Polym. Test. 55 (2016) 310–317.
[3] J. Odrobińska, K. Niesyto, K. Erfurt, A. Sieweniak, A. Mielańczyk, D. Neugebauer, Retinol-containing graft copolymers for delivery of skin-curing agents, Pharmaceutics 11 (8) (2019) 37.
[4] K. Kostrzewska, J. Ortyl, R. Dobosz, J. Kabatc, Squarylium dye and onium salts as highly sensitive photoradical generators for blue light, Polym. Chem. 8 (2017) 3464–3474.
[5] Y. Yagci, S. Jockusch, N.J. Turro, Photoinitiated polymerization: advances, challenges, and opportunities, Macromolecules 43 (2010) 6245–6260.
[6] P. Xiao, F. Dumur, B. Graff, J.P. Fouassier, D. Gigmes, J. Lalevée, Cationic and thiol–ene photopolymerization upon red lights using anthraquinone derivatives as photoinitiators, Macromolecules 46 (2013) 6744–6750.
[7] P. Glöckner, S. Struck, T. Jung, K. Studer, Radiation curing: coatings and printing inks: technical basics, applications and trouble shooting, Vincentz Network,, Hannover, 2008.
[8] P. Chang, H. Mei, S. Zhou, K.G. Dassios, L. Cheng, 3D printed electrochemical energy storage devices, J. Mater. Chem. A 7 (2019) 4230–4258.
[9] C. Yu, J. Schimelman, P. Wang, K.L. Miller, X. Ma, S. You, J. Guan, B. Sun, W. Zhu and S. Chen, *Chem. Rev.*, 120, **19**, 10695–10743.
[10] M. Topa, J. Ortyl, Materials (Basel), 13, 2020, p. 4093.
[11] J. Wang, A. Goyanes, S. Gaisford, A.W. Basit, Stereolithographic (SLA) 3D printing of oral modified-release dosage forms, Int. J. Pharm. 503 (2016) 207–212.
[12] M.O. Wang, C.E. Vorwald, M.L. Dreher, E.J. Mott, M.H. Cheng, A. Cinar, H. Mehdizadeh, S. Somo, D. Dean, E.M. Brey, J.P. Fisher, Evaluating 3D-printed biomaterials as scaffolds for vascularized bone tissue engineering, Adv. Mater. 27 (2014) 138–144.
[13] W. Tomal, J. Ortyl, Water-soluble photoinitiators in biomedical applications, Polymers 12 (2020) 1073.
[14] P. Zorlutuna, J.H. Jeong, H. Kong, R. Bashir, Stereolithography-based hydrogel microenvironments to examine cellular interactions, Adv. Funct. Mater. 21 (2011) 3642–3651.
[15] A. Bagheri, J. Jin, Photopolymerization in 3D printing, ACS Appl. Polym. Mater. 1 (2019) 593–611.
[16] K. Lee, N. Corrigan, C. Boyer, Rapid high-resolution 3D printing and surface functionalization via type i photoinitiated RAFT polymerization, Angew. Chem. - Int. Ed. 60 (2021) 8839–8850.
[17] J. Phommalysack-Lovan, Y. Chu, C. Boyer, J. Xu, PET-RAFT polymerisation: towards green and precision polymer manufacturing, Chem. Commun. 54 (2018) 6591–6606.
[18] W. Tomal, T. Świergosz, M. Pilch, W. Kasprzyk, J. Ortyl, New horizons for carbon dots: quantum nano-photoinitiating catalysts for cationic photopolymerization and three-dimensional (3D) printing under visible light, Polym. Chem. 12 (2021) 3661–3676.
[19] J. Olmsted, Calorimetric determinations of absolute fluorescence quantum yields, J. Phys. Chem. 83 (1979) 2581–2584.
[20] A. Bagheri, J. Jin, Photopolymerization in 3D printing, ACS Appl. Polym. Mater. 1 (2019) 593–611.
[21] M. Layani, X. Wang, S. Magdassi, Novel materials for 3D printing by photopolymerization, Adv. Mater. 30 (2018), e1706344.
[22] J. Zhang, P. Xiao, 3D printing of photopolymers, Polym. Chem. 9 (2018) 1530–1540.
[23] E. Hola, J. Ortyl, M. Jankowska, M. Pilch, M. Galek, F. Morlet-Savary, B. Graff, C. Dietlin, J. Lalevée, New bimolecular photoinitiating systems based on terphenyl derivatives as highly efficient photosensitizers for 3D printing application, Polym. Chem. 11 (2020) 922–935.
[24] S.C. Ligon, R. Liska, J. Stampfl, M. Gurr, R. Mülhaupt, Polymers for 3D printing and customized additive manufacturing, Chem. Rev. 117 (2017) 10212–10290.
[25] Z. Wang, W. Huang, P. Peng, D.E. Fennell, Rapid transformation of 1,2,3,4-TCDD by Pd/Fe catalysts, Chemosphere 78 (2010) 147–151.
[26] W. Tomal, M. Pilch, A. Chachaj-Brekiesz, M. Galek, F. Morlet-Savary, B. Graff, C. Dietlin, J. Lalevée, J. Ortyl, Photoinitiator-catalyst systems based onmeta-terphenyl derivatives as photosensitisers of iodonium and thianthrenium salts for visible photopolymerization in 3D printing processes, Polym. Chem. 11 (2020) 4604–4621.
[27] A. Kalkal, S. Kumar, P. Kumar, R. Pradhan, M. Willander, G. Packirisamy, S. Kumar, B.D. Malhotra, Addit. Manuf. 46 (2021), 102088.
[28] K. Jung, N. Corrigan, M. Ciftci, J. Xu, S.E. Seo, C.J. Hawker, C. Boyer, Designing with light: advanced 2D, 3D, and 4D materials, Adv. Mater. 32 (2020), 1903850.
[29] M. Layani, X. Wang, S. Magdassi, Novel materials for 3D printing by photopolymerization, Adv. Mater. 30 (2018), 1706344.
[30] F. Ondreas, P. Lepcio, M. Zboncak, K. Zarybnicka, L.E. Govaert, J. Jancar, Effect of nanoparticle organization on molecular mobility and mechanical properties of polymer nanocomposites, Macromolecules 52 (2019) 6250–6259.
[31] M. Zboncak, F. Ondreas, V. Uhlir, P. Lepcio, J. Michalicka, J. Jancar, Translation of segment scale stiffening into macroscale reinforcement in polymer nanocomposites, Polym. Eng. Sci. 60 (2020) 587–596.
[32] J. Jancar, F. Ondreas, P. Lepcio, M. Zboncak, K. Zarybnicka, Mechanical properties of glassy polymers with controlled NP spatial organization, Polym. Test. 90 (2020), 106640.
[33] W. Tomal, D. Krok, A. Chachaj-Brekiesz, J. Ortyl, Beneficial stilbene-based derivatives: from the synthesis of new catalytic photosensitizer to 3D printouts and fiber-reinforced composites, Eur. Polym. J. 156 (2021), 110603.
[34] W. Khan, R. Sharma, P. Saini, Carbon nanotubes: current progress of their polymer composites, in: M. Reda Berber, I. Hazzaa Hafez (Eds.), Carbon Nanotube-Based Polymer Composites: Synthesis, Properties and Applications, 1 edition.,, InTech, Rijeka, 2016, pp. 1–46.
[35] F.D.C. Siacor, Q. Chen, J.Y. Zhao, L. Han, A.D. Valino, E.B. Taboada, E.B. Caldona, R.C. Advincula, Addit. Manuf. 45 (2021), 102043.
[36] M. Sadej, H. Gojzewski, E. Andrzejewska, Photocurable polymethacrylate-silica nanocomposites: correlation between dispersion stability, curing kinetics, morphology and properties, J. Polym. Res. 23 (2016) 116.
[37] H. Gojzewski, M. Sadej, E. Andrzejewska, M. Kokowska, Nanoscale Young's modulus and surface morphology in photocurable polyacrylate/nanosilica composites, Eur. Polym. J. 88 (2017) 205–220.
[38] H. Gojzewski, M. Sadej, E. Andrzejewska, M. Kokowska, Dataset for acrylate/silica nanoparticles formulations and photocured composites: Viscosity, filler dispersion and bulk Poisson's ratio, Data Br. 12 (2017) 528–534.
[39] M. Sadej-Bajerlain, H. Gojzewski, E. Andrzejewska, Monomer/modified nanosilica systems: photopolymerization kinetics and composite characterization, Polym. (Guildf.). 52 (2011) 1495–1503.
[40] M. Sadej, E. Andrzejewska, Silica/aluminum oxide hybrid as a filler for photocurable composites, Prog. Org. Coat. 94 (2016) 1–8.
[41] Y.-Y. Wang, T.-E. Hsieh, Preparation and properties of polyacrylate/clay photocured nanocomposite materials, Chem. Mater. 17 (2005) 3331–3337.
[42] S.M. Sapuan, N. Bin Yusoff, Manufacturing of Natural Fibre Reinforced Polymer Composites, Springer International Publishing,, 2015, pp. 1–15.
[43] E. Andrzejewska, M. Andrzejewski, J. Jęczalik, T. Sterzyński, Polim./Polym. 54 (2009) 382–385.
[44] S.S. Alghamdi, S. John, N.R. Choudhury, N.K. Dutta, Effect of filler particle size on the recyclability of fly ash filled HDPE composites, Polymers 13 (2021) 1–39.
[45] Y. Zhang, Y. Xu, A. Simon-Masseron, J. Lalevée, Radical photoinitiation with LEDs and applications in the 3D printing of composites, Chem. Soc. Rev. 50 (2021) 3824–3841.
[46] A.C. De Leon, Q. Chen, N.B. Palaganas, J.O. Palaganas, J. Manapat, R.C. Advincula, High performance polymer nanocomposites for additive manufacturing applications, React. Funct. Polym. 103 (2016) 141–155.
[47] A. Chiappone, E. Fantino, I. Roppolo, M. Lorusso, D. Manfredi, P. Fino, C.F. Pirri, F. Calignano, 3D printed PEG-based hybrid nanocomposites obtained by sol-gel technique, ACS Appl. Mater. Interfaces 8 (2016) 5627–5633.
[48] J. Yang, C.R. Han, J.F. Duan, F. Xu, R.C. Sun, Mechanical and viscoelastic properties of cellulose nanocrystals reinforced poly(ethylene glycol) nanocomposite hydrogels, ACS Appl. Mater. Interfaces 5 (2013) 3199–3207.
[49] P. Lepcio, F. Ondreáš, K. Zárybnická, M. Zbončák, J. Svatík, J. Jančář, Phase diagram of bare particles in polymer nanocomposites: Uniting solution and melt blending, Polymer 230 (2021), 124033.
[50] K. Zarybnicka, F. Ondreas, P. Lepcio, M. Kalina, M. Zboncak, J. Jancar, Thermodynamic parameters controlling nanoparticle spatial packing in polymer solutions, Macromolecules 53 (2020) 8704–8713.
[51] Pilch Tomal, Chachaj-Brekiesz, Ortyl, Development of new high-performance biphenyl and terphenyl derivatives as versatile photoredox photoinitiating systems and their applications in 3D printing photopolymerization processes, Catalysts 9 (2019) 827.
[52] W. Tomal, A. Chachaj-Brekiesz, R. Popielarz, J. Ortyl, Multifunctional biphenyl derivatives as photosensitisers in various types of photopolymerization processes, including IPN formation, 3D printing of photocurable multiwalled carbon nanotubes (MWCNTs) fluorescent composites, RSC Adv. 10 (2020) 32162–32182.

[53] S. Mubarak, D. Dhamodharan, M.B. Kale, N. Divakaran, T. Senthil, S. P, L. Wu, J. Wang, A novel approach to enhance mechanical and thermal properties of SLA 3D printed structure by incorporation of metal–metal oxide nanoparticles, Nanomater 10 (2020) 217.
[54] L. Pezzana, G. Riccucci, S. Spriano, D. Battegazzore, M. Sangermano, A. Chiappone, 3D printing of PDMS-like polymer nanocomposites with enhanced thermal conductivity: boron nitride based photocuring system, Nanomater 11 (2021) 373.
[55] J. Wang, A. Chiappone, I. Roppolo, F. Shao, E. Fantino, M. Lorusso, D. Rentsch, K. Dietliker, C.F. Pirri, H. Grützmacher, All-in-one cellulose nanocrystals for 3D printing of nanocomposite hydrogels, Angew. Chem. Int. Ed. 57 (2018) 2353–2356.
[56] G. Gonzalez, A. Chiappone, I. Roppolo, E. Fantino, V. Bertana, F. Perrucci, L. Scaltrito, F. Pirri, M. Sangermano, Retraction: oncogenic activity of Cdc6 through repression of the INK4/ARF locus, Polymers (Guildf.). 109 (2017) 246–253.
[57] J. Zhang, F. Dumur, P. Xiao, B. Graff, D. Gigmes, J.P. Fouassier, J. Lalevée, Aminothiazonaphthalic anhydride derivatives as photoinitiators for violet/blue LED-Induced cationic and radical photopolymerizations and 3D-Printing resins, J. Polym. Sci. Part A Polym. Chem. 54 (2016) 1189–1196.
[58] J. Zhang, F. Dumur, P. Xiao, B. Graff, D. Bardelang, D. Gigmes, J.P. Fouassier, J. Lalevée, Structure design of naphthalimide derivatives: toward versatile photoinitiators for near-UV/Visible LEDs, 3D printing, and water-soluble photoinitiating systems, Macromolecules 48 (2015) 2054–2063.
[59] A. Al Mousawi, F. Dumur, P. Garra, J. Toufaily, T. Hamieh, F. Goubard, T.-T. Bui, B. Graff, D. Gigmes, J.P. Fouassier, J. Lalevée, Azahelicenes as visible light photoinitiators for cationic and radical polymerization: Preparation of photoluminescent polymers and use in high performance LED projector 3D printing resins, J. Polym. Sci. Part A Polym. Chem. 55 (2017) 1189–1199.
[60] F. Dumur, Recent advances on carbazole-based photoinitiators of polymerization, Eur. Polym. J. 125 (2020), 109503.
[61] J.H. Lee, R.K. Prud'homme, I.A. Aksay, Cure depth in photopolymerization: experiments and theory, J. Mater. Res. 16 (2001) 3536–3544.
[62] A. Abedini, E. Saion, F. Larki, A. Zakaria, M. Noroozi, N. Soltani, Room temperature radiolytic synthesized Cu@CuAlO(2)-Al(2)O(3) nanoparticles, Int. J. Mol. Sci. 13 (2012) 11941–11953.
[63] P.F. Jacobs, R*apid Prototyping & Manufacturing: Fundamentals of Stereolithography*. Society of Manufacturing Engineers, Dearborn,, 1992.
[64] J. Bennett, Addit. Manuf. 18 (2017) 203–212.
[65] A.C. Uzcategui, A. Muralidharan, V.L. Ferguson, S.J. Bryant, R.R. McLeod, Understanding and improving mechanical properties in 3D printed parts using a dual-cure acrylate-based resin for stereolithography, Adv. Eng. Mater. 20.12 (2018), 1800876.
[66] P.P. Romańczyk, S.S. Kurek, The reduction potential of diphenyliodonium polymerisation photoinitiator is Not −0.2 V vs. SCE. A computational study, Electrochim. Acta 255 (2017) 482–485.
[67] B. Strehmel, Application of NIR-photopolymers in the graphic industry: from physical chemistry to lithographic applications, Z. Phys. Chem. 228 (2014) 129–153.
[68] K.M.F. Shahil, A.A. Balandin, Graphene-multilayer graphene nanocomposites as highly efficient thermal interface materials, Nano Lett. 12 (2012) 861–867.
[69] H. Li, H. Liu, J. Li, D. Wei, Y. Wang, B. Song, Dielectric behaviors of carbon nanotube/silicone elastomer composites, Sci. Eng. Compos. Mater. 22 (2015) 215–221.
[70] C.K. Mytafides, L. Tzounis, G. Karalis, P. Formanek, A.S. Paipetis, High-power all-carbon fully printed and wearable SWCNT-based organic thermoelectric generator, ACS Appl. Mater. Interfaces 13 (2021) 11151–11165.
[71] G. Karalis, L. Tzounis, E. Dimos, C.K. Mytafides, M. Liebscher, A. Karydis-Messinis, N.E. Zafeiropoulos, A.S. Paipetis, Printed single-wall carbon nanotube-based joule heating devices integrated as functional laminae in advanced composites, ACS Appl. Mater. Interfaces 13 (2021) 39880–39893.
[72] Q. Mu, L. Wang, C.K. Dunn, X. Kuang, F. Duan, Z. Zhang, H.J. Qi, T. Wang, Addit. Manuf. 18 (2017) 74–83.
[73] P. Lepcio, F. Ondreas, K. Zarybnicka, M. Zboncak, O. Caha, J. Jancar, Bulk polymer nanocomposites with preparation protocol governed nanostructure: the origin and properties of aggregates and polymer bound clusters, Soft Matter 14 (2018) 2094–2103.